UCRL 1880

UNCLASSIFIED

UNIVERSITY OF CALIFORNIA

Radiation Laboratory

TWO-WEEK LOAN COPY

This is a Library Circulating Copy which may be borrowed for two weeks. For a personal retention copy, call Tech. Info. Division, Ext. 5545

BERKELEY, CALIFORNIA

DISCLAIMER

This document was prepared as an account of work sponsored by the United States Government. While this document is believed to contain correct information, neither the United States Government nor any agency thereof, nor the Regents of the University of California, nor any of their employees, makes any warranty, express or implied, or assumes any legal responsibility for the accuracy, completeness, or usefulness of any information, apparatus, product, or process disclosed, or represents that its use would not infringe privately owned rights. Reference herein to any specific commercial product, process, or service by its trade name, trademark, manufacturer, or otherwise, does not necessarily constitute or imply its endorsement, recommendation, or favoring by the United States Government or any agency thereof, or the Regents of the University of California. The views and opinions of authors expressed herein do not necessarily state or reflect those of the United States Government or any agency thereof or the Regents of the University of California.

UCRL-1880
Unclassified-Instrumentation

UNIVERSITY OF CALIFORNIA
Radiation Laboratory
Berkeley, California

Contract No. W-7405-eng-48

A FAST COUNTING SYSTEM FOR HIGH-ENERGY PARTICLE MEASUREMENTS

Richard Madey

October 1954

Printed for the U. S. Atomic Energy Commission

A FAST COUNTING SYSTEM FOR HIGH-ENERGY PARTICLE MEASUREMENTS

Contents

Abstract 3

I. Introduction 4

II. Pulse Shaping 8

III. Coincidence Circuit 34

IV. Output Circuits 50

V. Over-all Performance of the Coincidence System 54

Acknowledgments 61

References 62

A FAST COUNTING SYSTEM FOR HIGH-ENERGY PARTICLE MEASUREMENTS

Richard Madey†

Radiation Laboratory, Department of Physics
University of California, Berkeley, California

October 1954

ABSTRACT

A fast coincidence counting system for high-energy particle measurements combines a scintillation counter pulse-shaping circuit and a crystal diode coincidence circuit. The system is simple and reliable. Both the resolution time of the system and the double pulse separation time of the individual counters can be as short as three millimicroseconds, with essentially one hundred percent detection efficiency.

† Now at Brookhaven National Laboratory.

A FAST COUNTING SYSTEM FOR HIGH-ENERGY PARTICLE MEASUREMENTS

Richard Madey†

Radiation Laboratory, Department of Physics
University of California, Berkeley, California

October 1954

I. INTRODUCTION

The finite time interval between the production and the detection of a nuclear event may be used in various ways to discriminate against background. For example, experimental arrangements have been set up to select particles of a definite velocity. Scintillation-counter velocity selectors usually consist of two scintillation phosphors P 1 and P 2, a piece of transmission line, and a short-resolving-time coincidence circuit, arranged as shown in Fig. 1. Particles produced in the target with velocity v are detected when the particle flight time t_f between phosphors P 1 and P 2 is equal to the P 1 pulse-propagation time t_p for the particular length L of delay line used. Different velocities are selected by varying the length L of the delay line. For a given coincidence-circuit resolution time τ, good resolution in particle velocity v requires large distances d; on the other hand, since the P 1 scintillation phosphor is usually quite close to the target, the solid-angle factor causes the counting rate to fall off essentially as the inverse square of the distance d. Thus, such a velocity selector is most useful when there is a large flux of particles. For a given velocity resolution, the spacing d between the phosphors can be decreased as the resolving time of the coincidence circuit is decreased.

The disadvantage of small solid angle that is encountered in the usual application of the scintillation-counter velocity selector can be

† Now at Brookhaven National Laboratory.

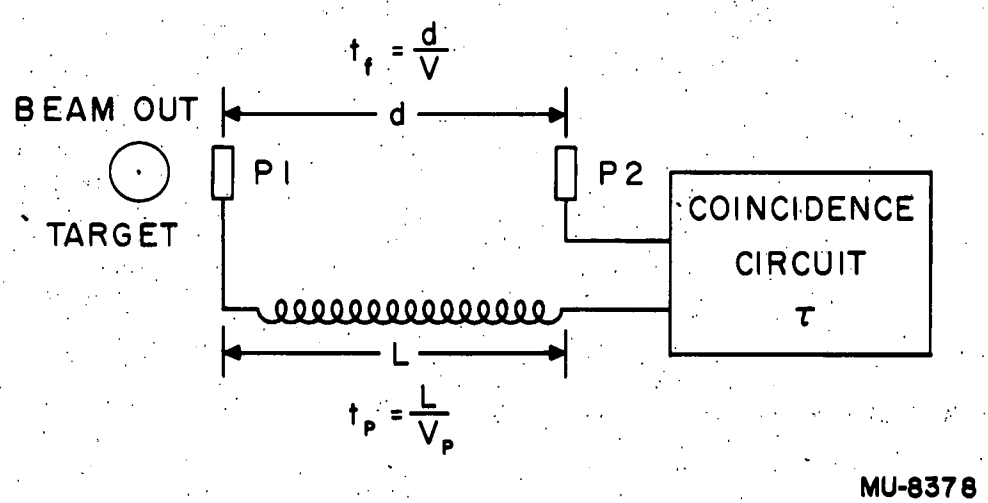

Fig. 1. A scintillation counter velocity selector.

overcome in some applications by taking advantage of the kinematical angular correlation properties of that class of two-body nuclear reactions in which a light and a heavy particle are produced in the final state. If both final-state particles are detected in coincidence, the kinematical angular correlation properties for such processes permit a velocity measurement of the heavy particle without loss of the solid angle. The reaction[1] $p + d \rightarrow \pi^+ + t$ will be used to illustrate this point. For such a two-body process, the equations for the conservation of energy and momentum can be solved to give the correlated angles and energies of the resultant particles. These angles and energies are shown in Fig. 2 for a bombarding proton energy of 340 Mev. A dominant feature of the kinematical angular correlation curve is the fact that tritons are confined within a twelve-degree cone about the beam axis. For the right half of the angular correlation curve in Fig. 2, a 9° angular interval for tritons in the center-of-mass system is compressed on the average into a 1° interval in the laboratory system; in the same transformation, the pion angular interval is changed only slightly. If the distance of the triton detector from the target is nine times that of the pion detector, then triton and pion detectors of the same horizontal dimensions will subtend the same angular interval in the center-of-mass system. Even though the triton detector is considerably farther from the target than the pion detector, both detectors will be about the same perpendicular distance from the beam axis; therefore, triton and pion detectors of roughly the same vertical dimensions will intercept the same azimuthal angular interval. Thus, the solid angle determined by the pion detector at a relatively small distance from the target is not reduced if the triton detector is at a relatively large distance from the target. This large distance of the triton detector from the target permits a time-of-flight measurement of the triton velocity.

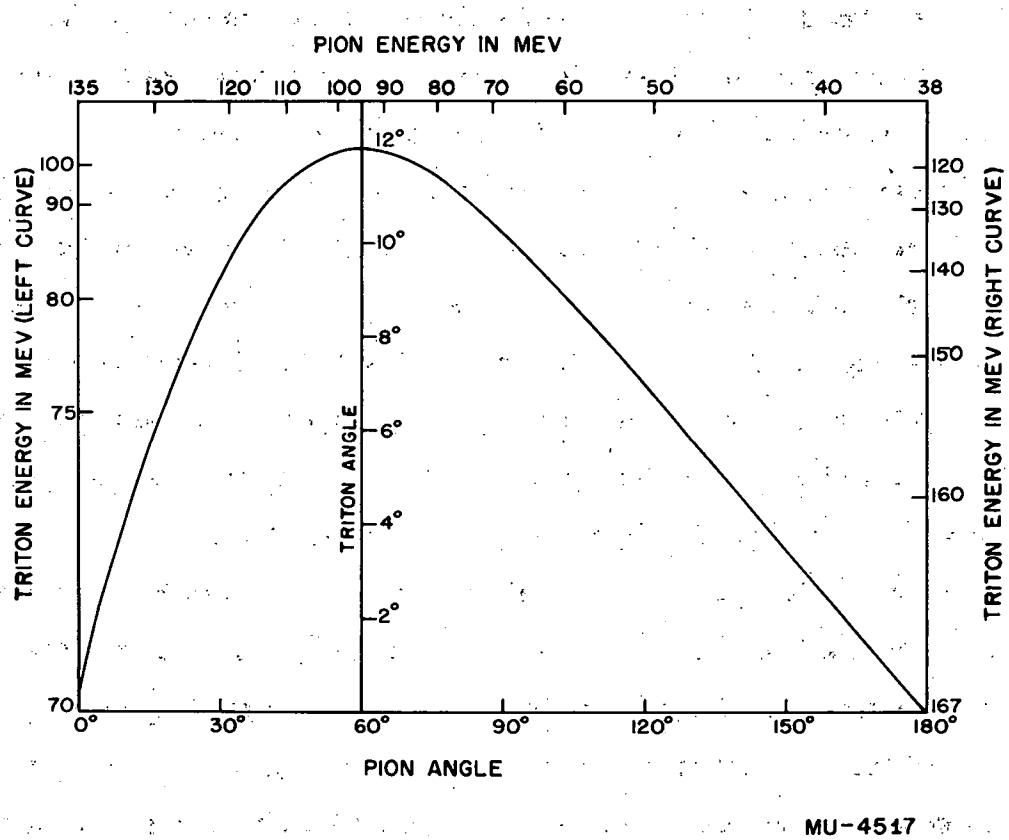

Fig. 2. Correlated angles and energies in the laboratory system for the process $p + d \rightarrow \pi^+ + t$. The incident proton energy is 340 Mev.

II. PULSE SHAPING

The "dead" time in the scintillation counter external circuitry can place limitations on the performance of the velocity selector in the presence of a large number of background particles. The dead time of the counter is defined here as the time that can elapse between responses of the counter to successive pulses. The origin of the dead time of a scintillation counter can be visualized from an equivalent circuit representation of the counter. The scintillation phosphor and photomultiplier combination is represented in Fig. 3 as a pulse generator with an internal impedance that is large compared to the load impedance; furthermore, the internal impedance is allowed to be variable in order to represent different amounts of energy loss in the scintillation phosphor. If the RC time constant of the load impedance is small compared to the decay time of the scintillator, then the voltage pulse at the output of the photomultiplier will decay in a time that is characteristic of the material of the scintillator. The rise time of the voltage pulse at the output of the photomultiplier tube is limited by the spread of the time of flight of electrons in the tube. The transit-time spread means that electrons descended from the same photon do not enter the collecting space simultaneously. For the purpose of the following discussion, we will assume that the voltage pulse at the output of the photomultiplier tube rises sharply in a time of the order of one millimicrosecond and decays exponentially with the characteristic decay time of the scintillator. A typical 1/e - decay time for a trans-stilbene phosphor is about eight millimicroseconds.[2] Characteristic decay times of some other scintillators are listed in Table I. Since the magnitudes of the current pulses that are delivered to the load impedance depend† upon the energy that

† Measurements of the relative response of scintillation phosphors to different particles have been reported in the literature. The most comprehensive investigation has been made by Taylor et al.[3] For further references, see the book by Birks.[4]

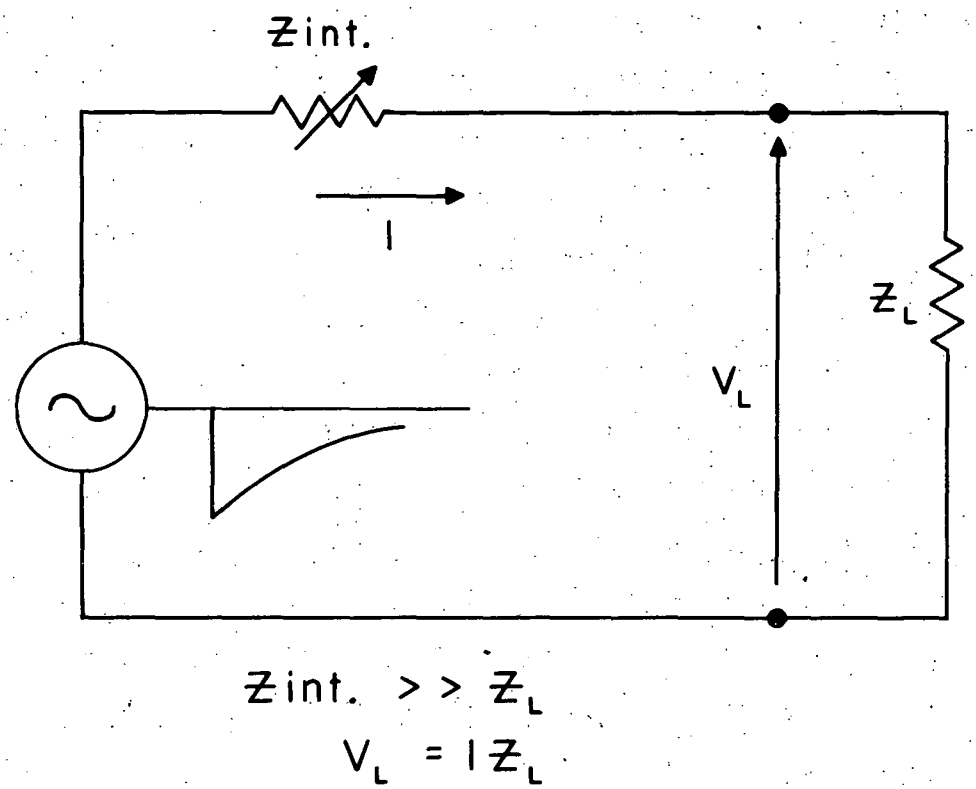

Fig. 3. An equivalent circuit of the scintillation counter.

is lost by a particle in passing through the scintillation phosphor, variations occur in the voltage amplitudes of the output pulses. Pulses of varying amplitudes require different periods of time to decay below a certain threshold value, specified as h* in Fig. 4. The time for the pulse amplitude to decay below this threshold amplitude is a measure of the dead time of the counter. Thus, a large dead time is associated with a pulse of large amplitude, and a small dead time is associated with a pulse of small amplitude. This correlation of the dead time with the pulse amplitude is illustrated in Fig. 4. Suppose a discriminator is adjusted so that the threshold amplitude h* is equal to 1/e times the peak amplitude of the smallest detectable pulse; then, Fig. 5 is a plot of peak pulse height h, against the time t*, for the pulse amplitude to decay exponentially to the threshold amplitude h*, where h is measured in units of the threshold amplitude h*, and t* is measured in units of the characteristic decay time τ of the scintillator. If t* is taken as a measure of the dead time of the counter, then the "dead" time increases by a factor of 1.7 for a peak pulse height equal to twice that of the smallest detectable pulse, by a factor of 2.4 for a peak pulse height four times as big, by a factor of 3.1 for one eight times as big, and by a factor of 3.8 for one sixteen times as big. The plotted relation in Fig. 5 is

$$t^*/\tau = 1 + \log_e h. \qquad (1)$$

Scintillation-counter pulses of both large and small amplitudes may be confined within the same definite time interval by using a coaxial transmission line, terminated in a short circuit or small impedance at its receiving end and in its characteristic impedance at its sending end, as part of the load impedance of the photomultiplier. A transmission line pulse-duration limiter circuit is illustrated schematically in Fig. 6. There is an optimum value of the terminating impedance for minimum overshoot in the resultant pulse. The optimum value depends on the characteristic impedance and the length of the clipping line and on the shape of the scintillation counter pulse. Maximum overshoot occurs for the

Table I

Characteristic Decay Times and other Properties
Of Some Fast Scintillation Phosphors

Name	Composition	H/C Ratio	Density g/cm^3	Reference	Index of Refraction	Reference	Decay Time mμsec	Reference
INORGANIC CRYSTAL								
Sodium Iodide	NaI(Tl)		3.67		1.7745		250	1
ORGANIC CRYSTAL								
Diphenylacetylene (Tolane)	$C_{14}H_{10}$	0.71	0.966	12			6.9	4
Trans-stilbene	$C_{14}H_{12}$	0.86	1.16	1	1.622		8.2	4
Anthracene	$C_{14}H_{10}$	0.71	1.25	1	1.595		29.4	4
LIQUID								
Terphenyl in Xylene [a]	C_8H_{10}	1.25	0.88009(o)	6	1.50516(o)	9		
			0.86415(m)	7	1.49717(m)	10	8.8(m)	3 [a]
			0.86102(p)	8	1.49583(p)	11	6.5(p)	3 [a]
Phenylcyclohexane [b]	$C_{12}H_{16}$	1.33	0.9431	5	1.5249	5	6.8	3
PLASTIC								
Pilot "B"		1.10	1.03	13	1.585	13	4	13

References for Table I

1. O. R. Frisch, Progress in Nuclear Physics, Vol. 2 (Academic Press, New York, 1952), p. 58.
2. H. Kallmann and M. Furst, Phys. Rev. 81, 858 (1951).
3. L. Bittman, M. Furst, and H. Kallmann, Phys. Rev. 87, 84 (1952).
4. H. B. Phillips and R. K. Swank, Rev. Sci. Instr. 24, 615 (1953).
5. Faraday, Encyclopedia of Hydrocarbon Compounds, Vol. 10 (Chemical Publishing Co., New York, 1954), p. 12111.00.14.
6. Faraday, op. cit. Vol. 3a, p. 08015.00.85.
7. Faraday, op. cit., p. 08016.00.86.
8. Faraday, op. cit., p. 08017.00.86.
9. Faraday, op. cit., p. 08015.00.88.
10. Faraday, op. cit., p. 08016.00.89.
11. Faraday, op. cit., p. 08017.00.90.
12. Lange, Handbook of Chemistry, 8th Ed. (Handbook Publishers, Sandusky, Ohio, 1952), p. 677.
13. Data from Pilot Chemicals, Inc., 47 Felton Street, Waltham 54 Massachusetts.

---

a Time constants given for xylene + p-terphenyl (5g/ℓ) and for xylene +m-terphenyl (200 g/ℓ).

b Kallmann mixture: phenylcyclohexane with 3 g/ℓ of terphenyl and 15 mg/ℓ of diphenylhexatriene. (Ref. 2).

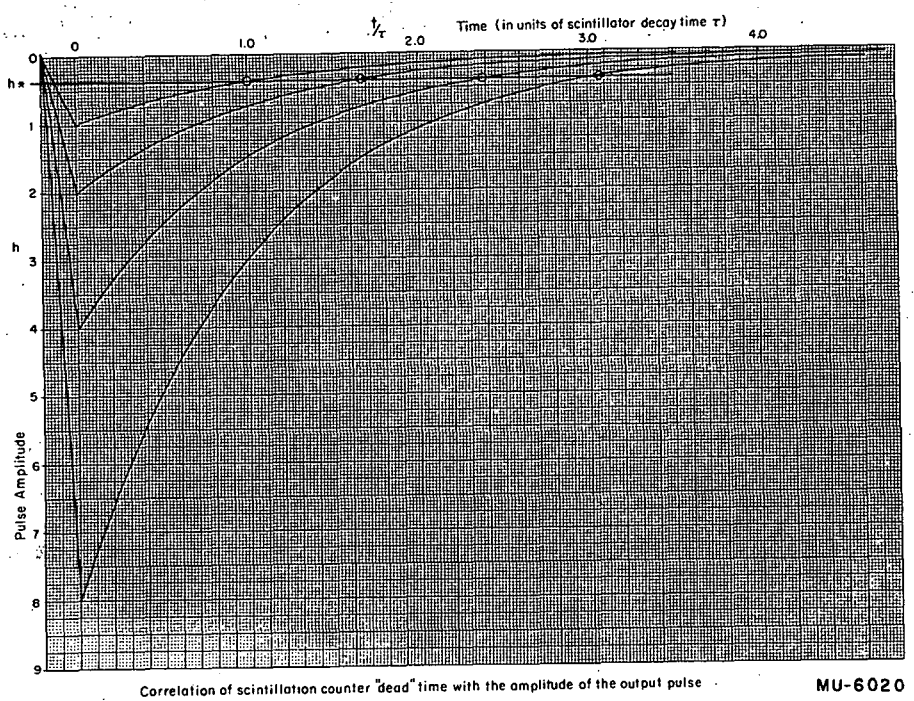

Fig. 4. Correlation of scintillation counter "dead" time with the amplitude of the output pulse.

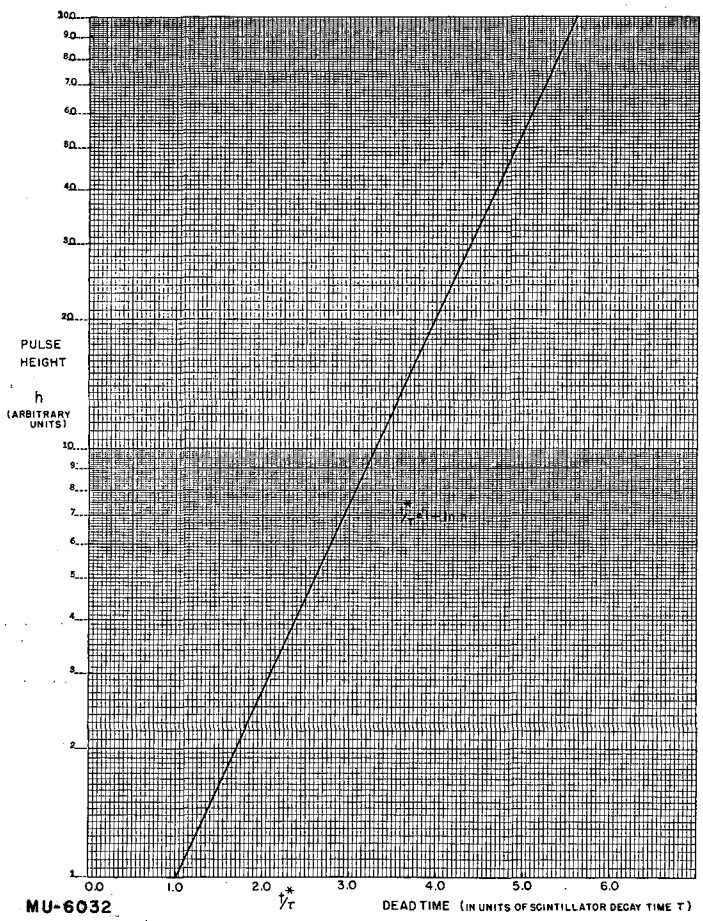

Fig. 5. Peak pulse height h versus the time t^* for the pulse amplitude to decay exponentially to an arbitrary threshold amplitude h^*, where h is measured in units of the threshold amplitude h^*, and t^* is measured in units of the characteristic decay time τ of the scintillator.

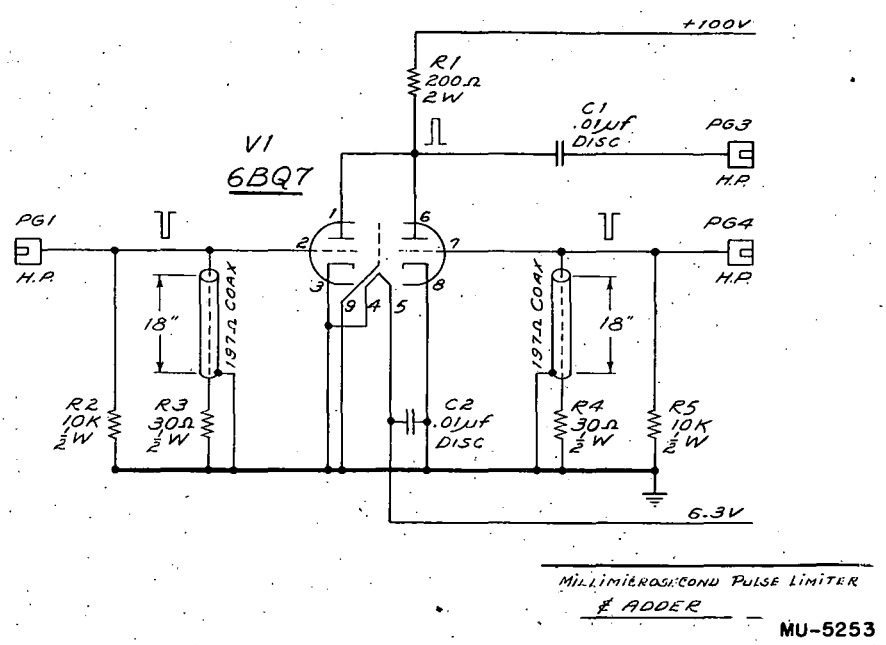

Fig. 6. A transmission-line type pulse-duration limiter for pulse durations in the millimicrosecond range.

short circuit termination because, in this case, all of the original peak amplitude is reflected. A terminating resistance that is some small fraction of the characteristic impedance of the line will absorb some of the energy in the incident pulse and will reflect back a fraction of the original peak amplitude. The proper terminating resistance reflects that fraction of the peak amplitude of the incident pulse which will just cancel the amplitude that the incident pulse has at a time equivalent to twice the length of the clipping line. Figure 7 illustrates the pulse shape for several values of the voltage reflection coefficient μ, where μ is the voltage of the reflected pulse divided by the voltage of the incident pulse. The reflection coefficient μ is related to the terminating impedance Z_t through the equation

$$Z_t/Z_o = (1 + \mu)/(1 - \mu), \tag{2}$$

where Z_o is the characteristic impedance of the coaxial line. Values of Z_t for some typical values of Z_o are given in Table II as a function of μ.

Table II

The Terminating Impedance Z_t as a Function of the Voltage Reflection Coefficient μ for Some Typical Values of the Coaxial Line Characteristic Impedance Z_o

μ	Z_t/Z_o	Z_t (ohms)					
		Z_o=950	259	197	185	171	125
0	1	950	259	197	185	171	125
-0.25	3/5	570	155	118	111	103	75
-0.50	1/3	317	86	66	62	57	42
-0.75	1/7	136	37	28	26	24	18
-1.00	0	0	0	0	0	0	0

Table III

Some Properties of Coaxial Cables

Manufacturer	Type	Characteristic Impedance (ohms)	Propagation Velocity				Delay Time	Attenuation in db/100 feet f(mc/sec)						
			β	cm per μsec	in. per μsec	ft. per μsec	μsec per ft. at 5 mc/s	10	100	200	300	400	600	1000
Federal	RG65/U	950 ± 50	.0242	.736	0.286	.0238	42	21.5	--	--	--	--	--	--
Transradio	C344-T	259	.953	28.6	11.2_4	.937	1.068	0.78	2.9	--	--	--	11.9	--
Transradio	C3-T	197	.953	28.6	11.2_4	.937	1.068	0.51	1.9	--	--	--	7.6	--
Amphenol	RG114/U	185	.86	25.8	10.1_6	.843	1.185	--	4.84	6.26	--	8.50	--	--
Transradio	C2-T	171	.942	28.2	11.1_0	.925	1.082	0.59	2.15	--	--	--	8.8	--
Amphenol	RG63/U	125	.84	25.2	9.9_2	.827	1.148	0.6	2.0	2.9	3.6	4.2	--	7.0

In Fig. 7, the photomultiplier output pulse is assumed to rise to its peak amplitude in one millimicrosecond and to decay exponentially to 1/e of peak amplitude in five millimicroseconds. The length of the clipping line is taken to be 1.5 millimicroseconds. In practice, the optimum value of terminating resistance is chosen experimentally.

Some properties of coaxial cables are given in Table III. The type RG 65/U cable is a special high-impedance delay-line cable that has a very slow propagation velocity. Other available coaxial cables have propagation velocities near that of light. For example, both the 197-ohm (Trans-radio type C3-T) and the 259-ohm (Trans-radio type 344-T) British cables propagate electromagnetic waves with a $\beta = v/c = 0.953$, or a velocity of 937 feet per microsecond, so that about 11 inches correspond to one millimicrosecond delay. Hence, if either of these cables is used in the transmission-line pulse-duration limiter, a delay-line clipping time smaller than one millimicrosecond should be possible; however, if the photomultiplier output current is not driven to its saturation value, the minimum scintillation counter "dead" time would be limited by the rise time of the scintillation counter pulse.

The photomultiplier load impedance Z_L in Fig. 8 consists of a parallel resistance-capacitance circuit. Since the sending end of the RG 65/U transmission line is terminated with a resistance equal to the characteristic impedance of the line, the value of the load resistance is equal to one-half the characteristic impedance Z_o of the delay line; the value of the capacitance C is equal to the sum of the input capacitance of the pulse-duration limiter tube, the capacitance of the collector of the photomultiplier, and the stray wiring capacitance. The photomultiplier load impedance Z_L is plotted as a function of frequency f in Fig. 9 for a characteristic impedance Z_o equal to 950 ohms, and for typical capacitance values of 3, 6, and 12 micromicrofarads. Figures 10 through 14 are

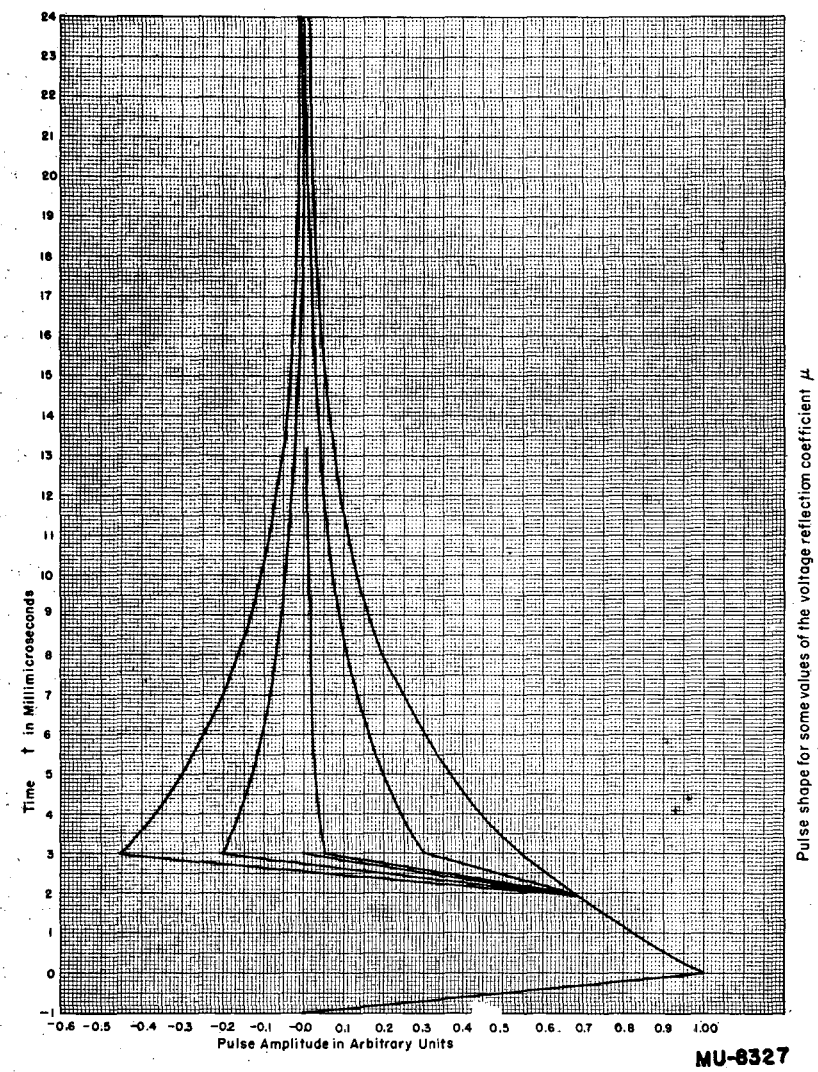

Fig. 7. Pulse shape versus voltage reflection coefficient μ.

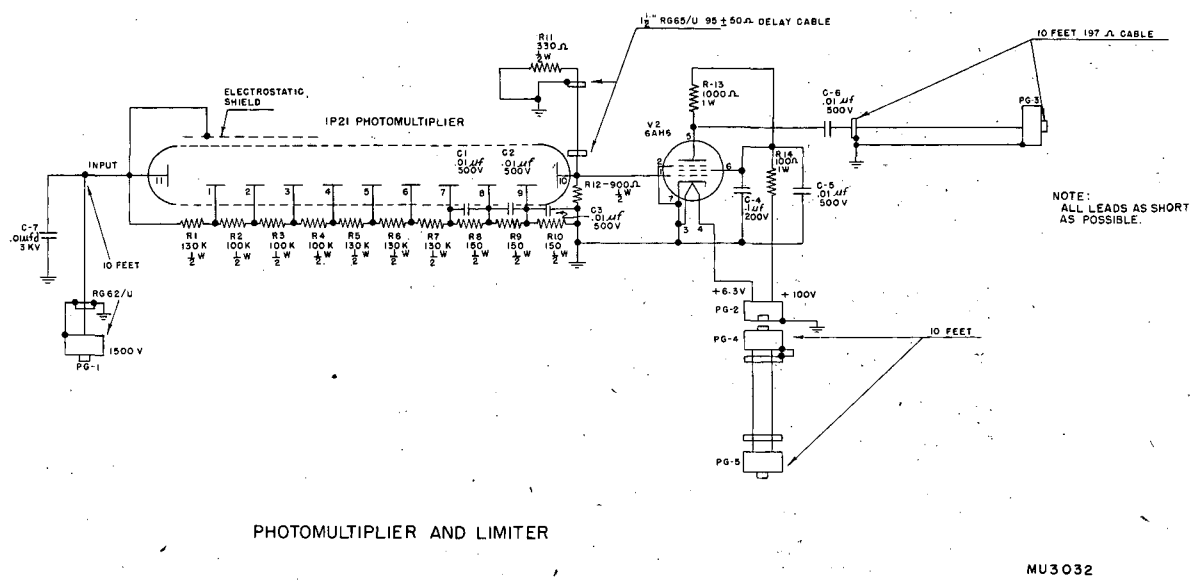

PHOTOMULTIPLIER AND LIMITER

Fig. 8. A transmission-line type pulse-duration limiter for pulse durations greater than about ten millimicroseconds.

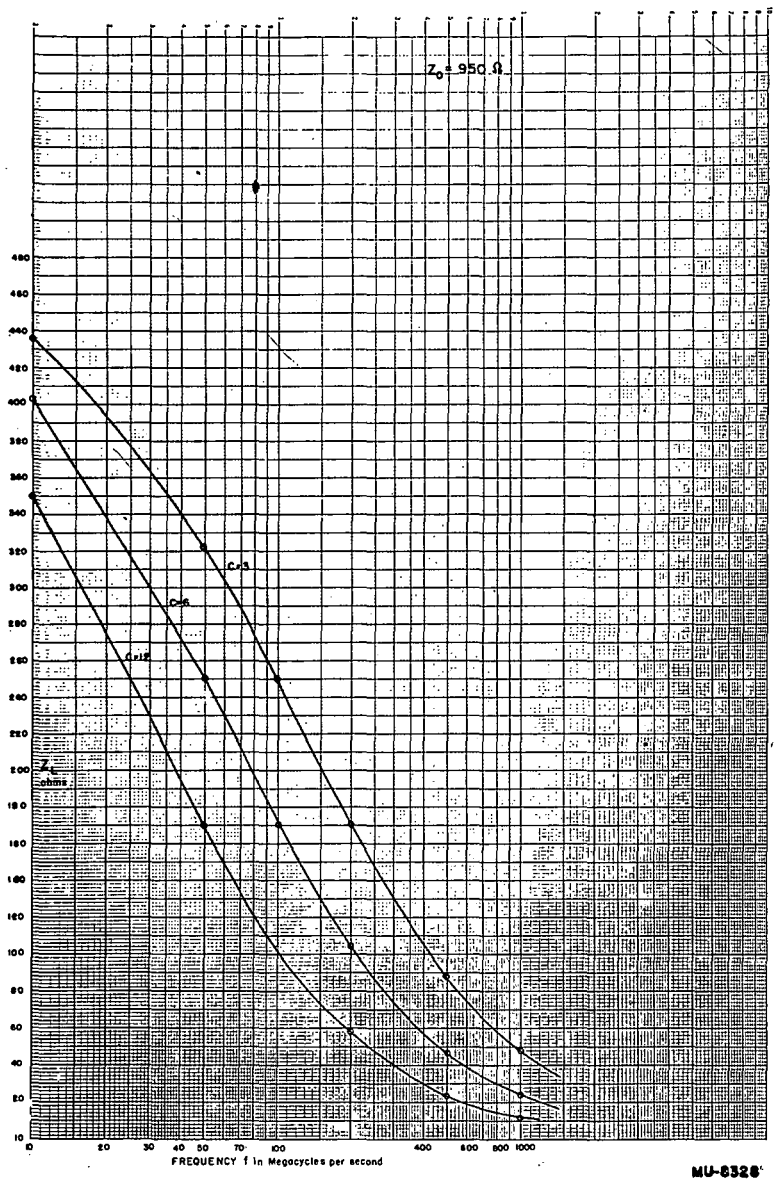

Fig. 9. The photomultiplier load impedance Z_L versus frequency f for a characteristic impedance Z_o of 950 ohms.

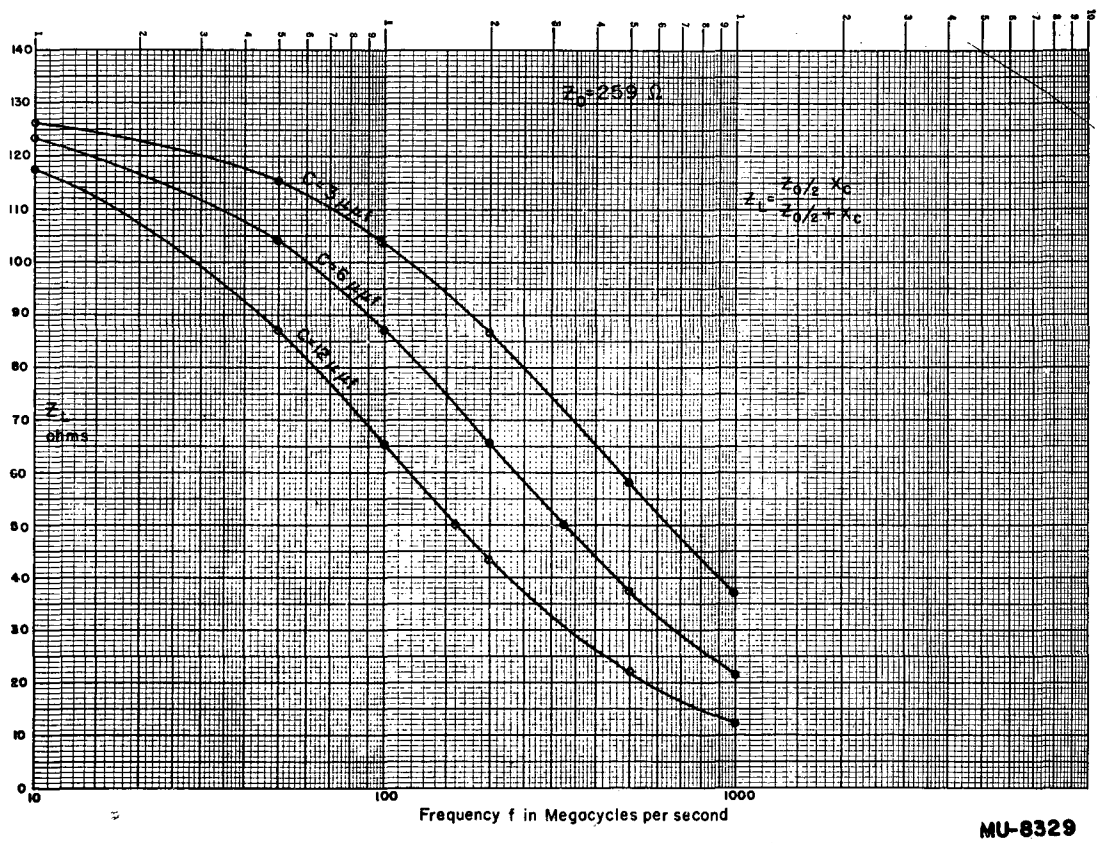

Fig. 10. The photomultiplier load impedance Z_L versus frequency f for a characteristic impedance Z_o of 259 ohms.

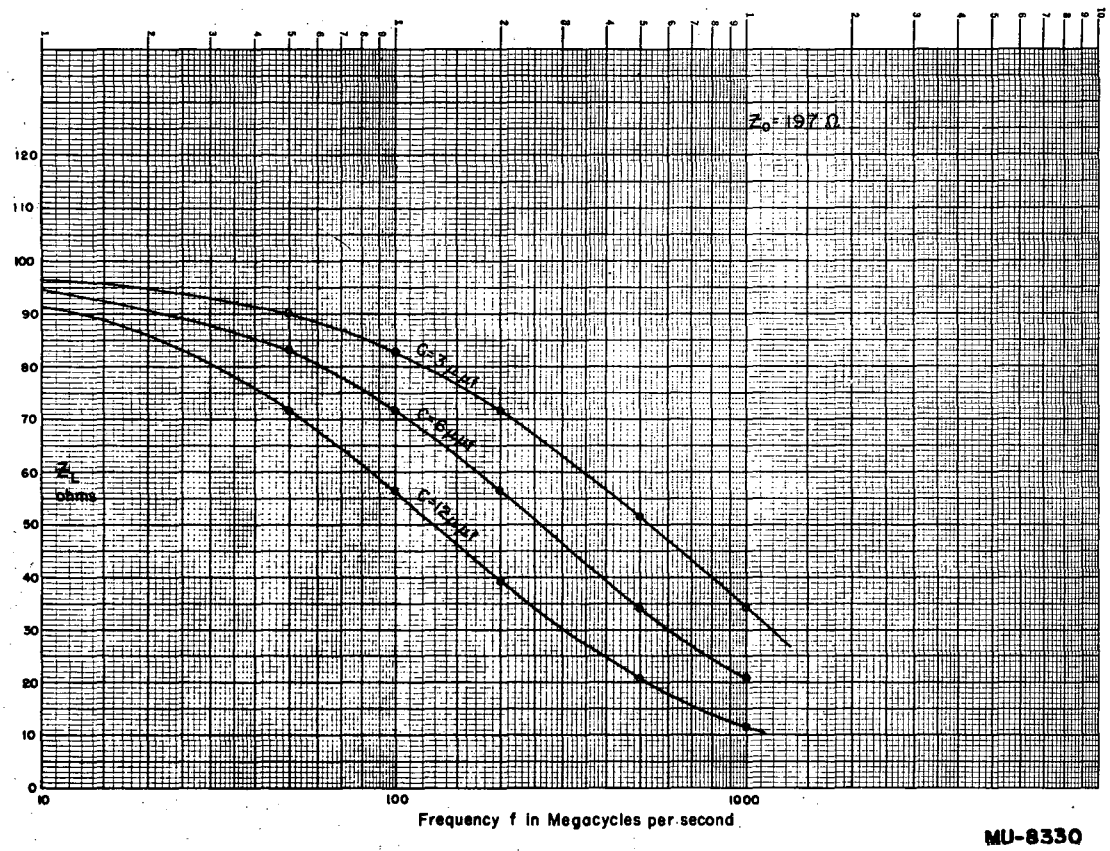

Fig. 11. The photomultiplier load impedance Z_L versus frequency f for a characteristic impedance Z_o of 197 ohms.

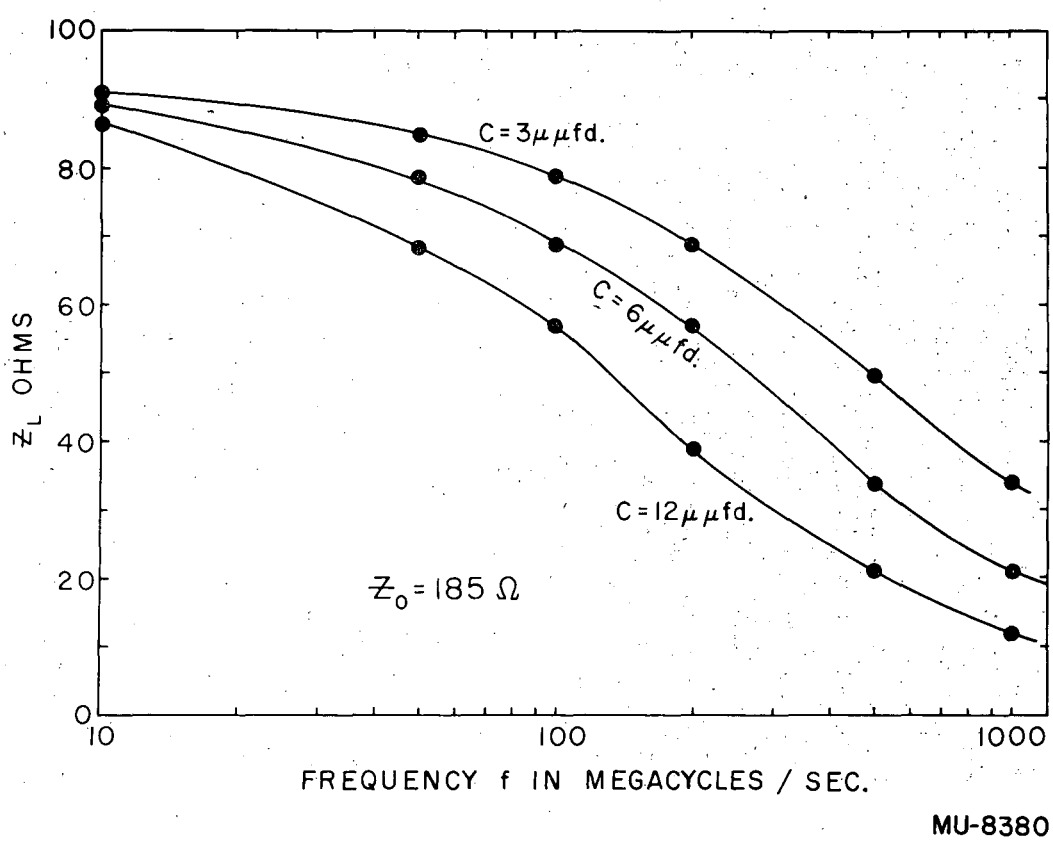

Fig. 12. The photomultiplier load impedance Z_L versus frequency f for a characteristic impedance Z_o of 185 ohms.

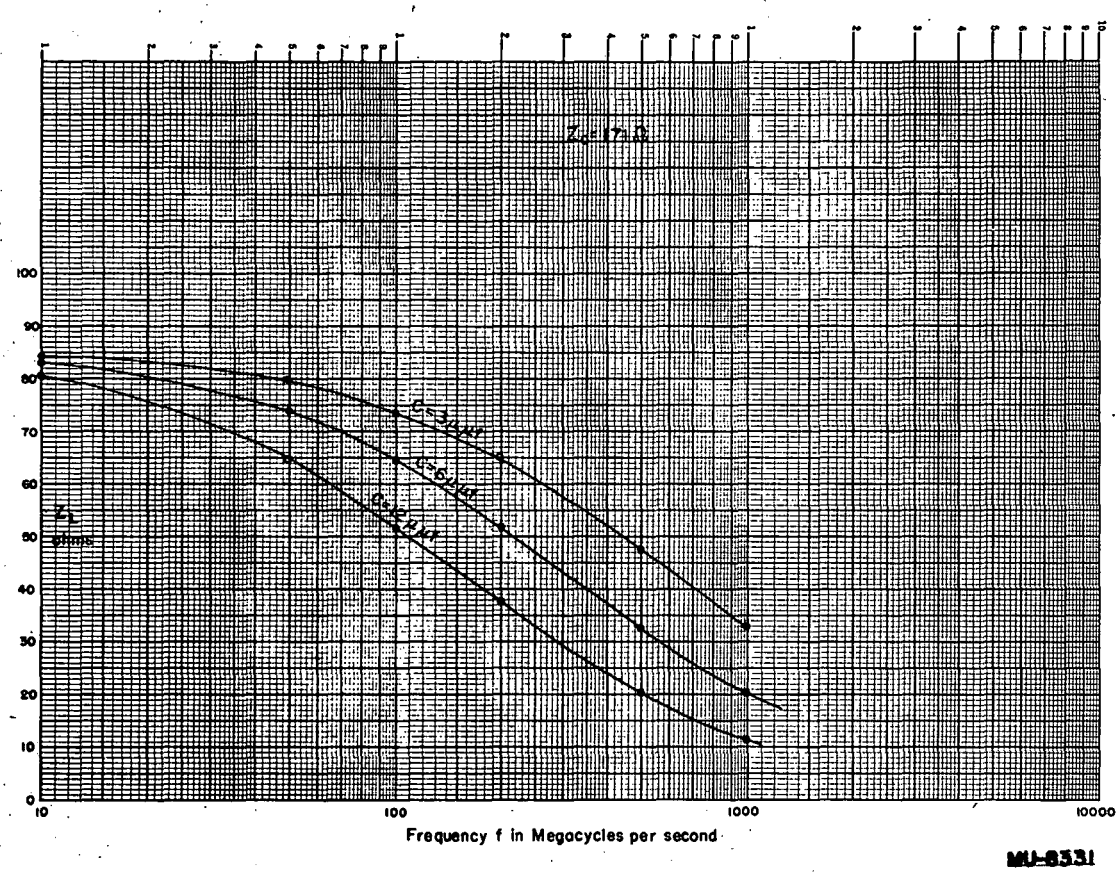

Fig. 13. The photomultiplier load impedance Z_L versus frequency f for a characteristic impedance Z_o of 171 ohms.

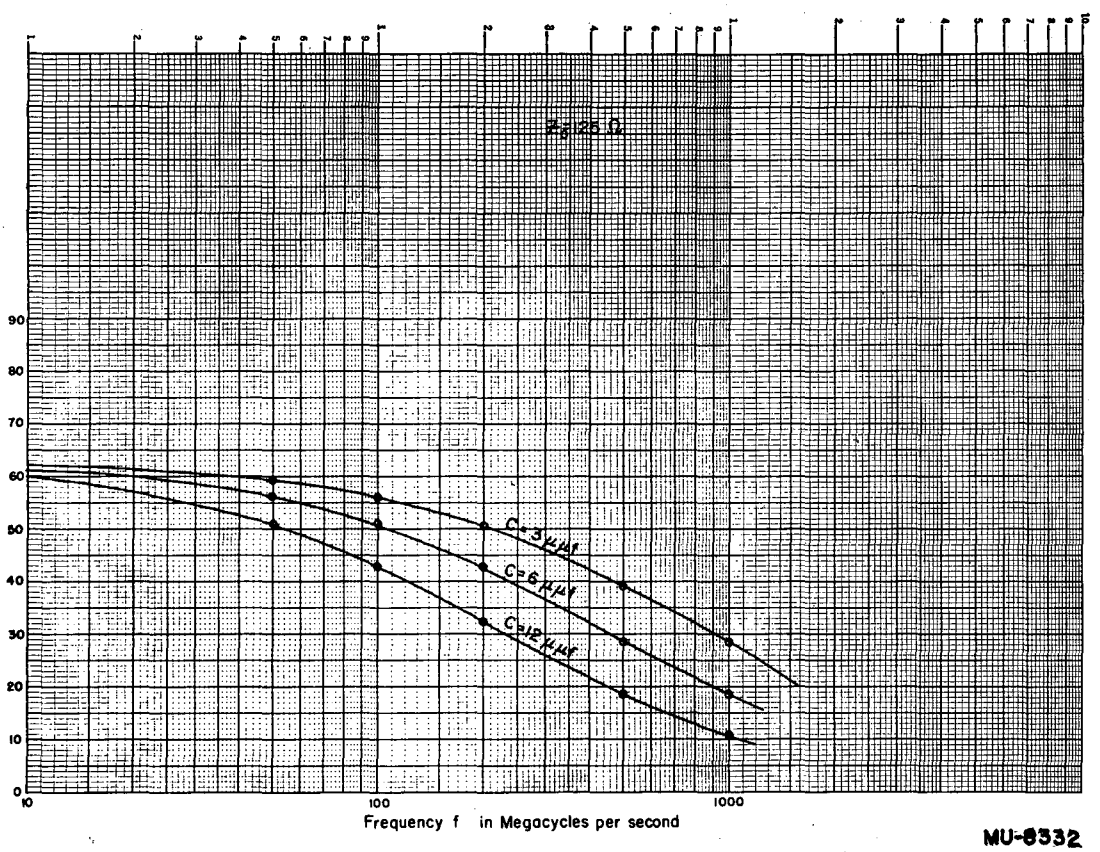

Fig. 14. The photomultiplier load impedance Z_L versus frequency f for a characteristic impedance Z_o of 125 ohms.

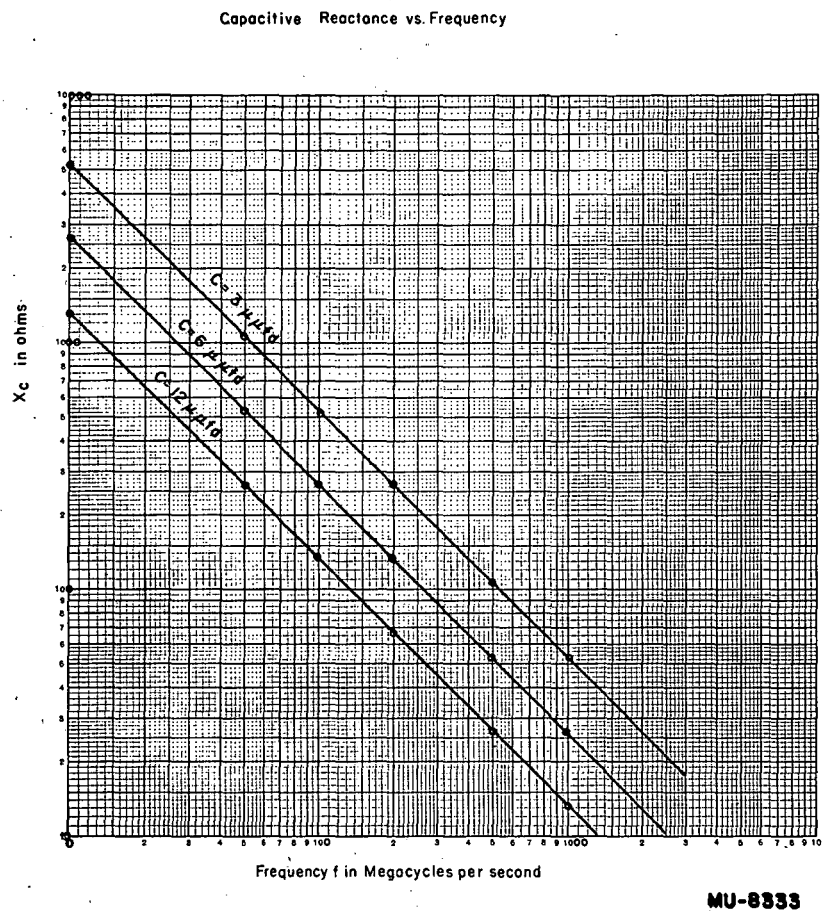

Fig. 15. Capacitive reactance versus frequency for capacitance values of 3, 6, 12 micromicrofarads.

similar plots for Z_o equal to 259, 197, 185, 171, and 125 ohms. The plotted relation is

$$Z_L = X_c (Z_o/2) / (X_c + Z_o/2),$$

where

$$X_c = 1/(2\pi fC).$$

The variation of the capacitive reactance with frequency for the same three capacitance values is plotted in Fig. 15 for comparison.

In the transmission line type of pulse-duration limiter of Fig. 8, the short length (1-1/2 inches) of high-impedance (950 ± 50 ohms) RG 65/U delay cable serves as the time clipper or dead-time equalizer for pulses of different amplitudes; however, a dead time smaller than about 10 milli-microseconds cannot be obtained with this delay cable because lengths smaller than about 1-1/2 inches no longer behave like a transmission line.

In the photomultiplier and pulse-duration limiter circuit of Fig. 6, the grid of the vacuum tube is connected somewhere near the receiving end of the transmission line instead of at the sending end as in Fig. 8. This change results in a more nearly resistive termination at the sending end of the transmission line. The pulse duration is determined by the distance along the cable, measured from the nearly short-circuited receiving end, at which the vacuum-tube grid is connected. The length of the nearly shorted transmission line in the photomultiplier pulse-shaping circuit of Fig. 6 is calculated to generate pulses of 3×10^{-9} seconds' duration at the base of the pulse.

Since the type 6BQ7A tube is a double triode, only one glass envelope is necessary to serve two photomultipliers. This fact suggests the possibility that short pulses from two photomultipliers can be applied to the input grids of the double triode and added together with a common plate-load impedance. If two photomultipliers view a common scintillator, uniform detection efficiency is obtainable over a large scintillator area.

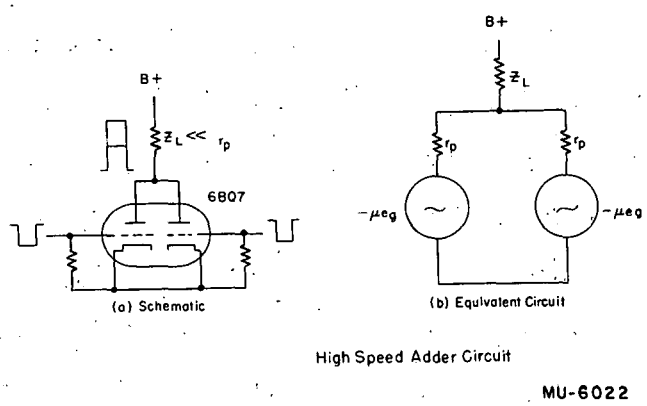

Fig. 16. High-speed adder circuit.
a. Schematic
b. Equivalent circuit

The schematic circuit diagram for the high-speed adder is given in Fig. 16a; the equivalent circuit in Fig. 16b. At first glance, the adder circuit appears to be the same as the well-known Rossi coincidence circuit;[5] the difference, however, is contained in the magnitude of the load impedance Z_L relative to the magnitude of the dynamic plate resistance r_p of either vacuum tube. For the coincidence circuit, the load impedance is much larger than the plate resistance; thus, the signal voltage at the common plate connection does not change appreciably unless both grids are actuated by coincident pulses. The plate-current change that results from the presence of only one grid pulse is prevented from developing a signal voltage across the load impedance by the clamping action of the other tube. For the high-speed adder circuit, the load impedance is much smaller than the plate resistance of either tube; thus, the plate-current change that results either from only one grid pulse or from two coincident grid pulses will develop a signal voltage across the load impedance. The large ratio of plate resistance to load impedance effectively isolates each tube from the other. The plate-load impedance for the high-speed adder circuit in Fig. 6 consists of 197-ohm line, terminated with a resistor equal to the characteristic impedance, in parallel with the output and the stray capacities of the plate circuit. The rise time of the pulses from the high-speed adder circuit are probably governed by grid loading and transit-time effects within the vacuum tube rather than by the time constants of the input and output circuits. The output time constant of the adder circuit is

$$\tau_{output} = \frac{Z_o}{2} \cdot C_{output}, \qquad (3)$$

where Z_o is the characteristic impedance of the plate line, and C_{output} is equal to the output capacitance of both sections of the 6BQ7A triode plus the stray wiring capacitance. Since the output capacitance of one section of the 6BQ7A triode is given as 1.35 micromicrofarads, the output time

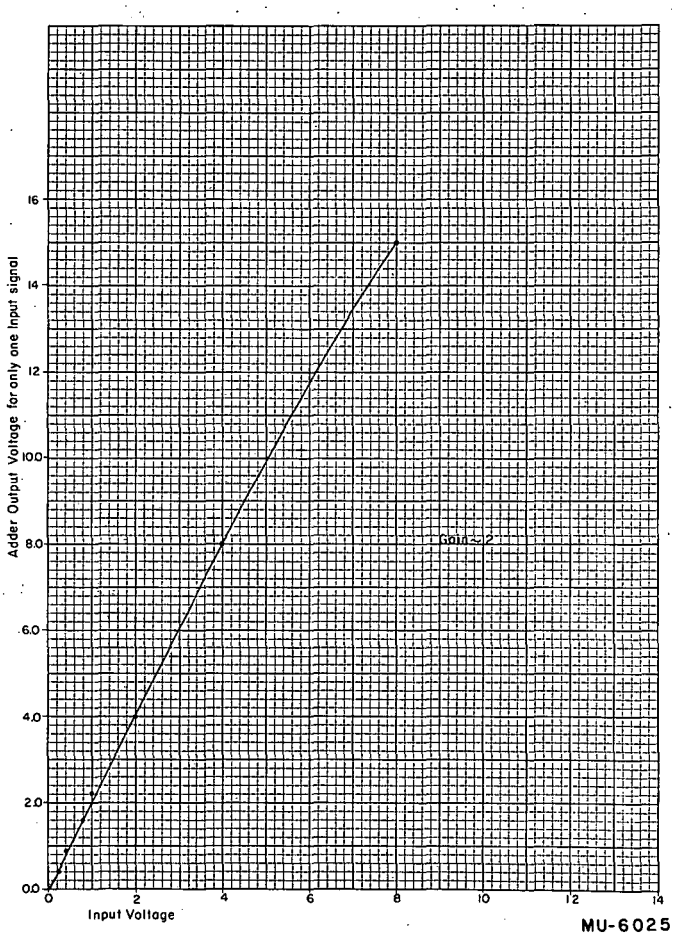

Fig. 17. The output voltage versus the input grid voltage on one input only to the high-speed adder. The input signals are ten-millimicrosecond square pulses of positive polarity.

constant is less than one millimicrosecond when 197-ohm line is used in the plate circuit. Since the input capacitance of one section of the 6BQ7 tube is given as 2.85 micromicrofarads, the input time constant is also probably less than one millimicrosecond if 197-ohm line is used in the grid circuit.

Although the 6BQ7 adder circuit is operated at zero grid bias, it may be driven by either negative or positive pulses. If the grids are driven negatively beyond the cutoff value of approximately two volts, the output pulse is limited in amplitude. An amplitude limiter is desirable, for example, in those experiments that are designed to detect lightly ionizing particles, such as electrons, in the presence of a large background of heavily ionizing particles, such as protons. On the other hand, if an experiment is designed to detect heavily ionizing particles in the presence of a large background of lightly ionizing particles, then no amplitude-limiting action is desired. Figure 17 shows that the output of the adder circuit is linear with the positive input signal on one of the grids; Fig. 18 gives the linear output-input relation when positive input pulses of the same amplitude are applied simultaneously to each grid. Both Fig. 17 and Fig. 18 show that the adder circuit has a voltage gain of about two for ten-millimicrosecond square input pulses.

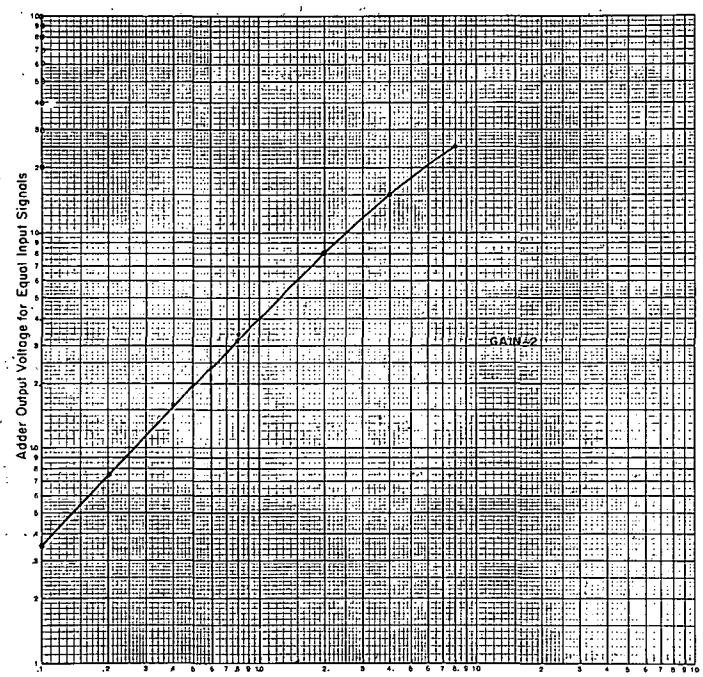

MU-6031

Fig. 18. The output voltage versus the amplitude of one of two equal-input grid voltage signals that are applied simultaneously to the high-speed adder. The input signals are ten-millimicrosecond square pulses of positive polarity.

III. COINCIDENCE CIRCUIT

The active components of the coincidence circuit consist entirely of crystal diodes. The principal advantage of using crystal diodes instead of vacuum tubes for mixing the input pulses is that the diode circuit can be driven directly either from 1P21 photomultiplier tubes or from the high-speed limiter-adder circuit of Fig. 16 without the aid of distributed amplification. Since the rise time of scintillation-counter pulses is believed to be smaller than the rise time of commercially available distributed amplifiers, the scintillation-counter pulse is degraded slightly in passing through a distributed amplifier that has a rise time of about 2.5 millimicroseconds. Thus, in addition to the obvious advantages of simplicity, lower cost, and less electronic maintenance, the main advantage sought in the elimination of distributed amplifiers was the ability to drive the coincidence circuit with pulses of the shortest possible duration.

Figure 19 is a schematic circuit diagram of one version of the coincidence circuit; namely, a double-coincidence circuit that operates on positive input pulses. If the polarities of all the crystal diodes and both bias supplies are reversed, then the double-coincidence circuit will operate on negative input pulses. A schematic of such a circuit is given in Fig. 20. Slight modifications can be made to Figs. 19 and 20 in order to allow both positive and negative input circuits to operate from a single commercially available 150-volt power supply. Circuit diagrams are shown in Figs. 21 and 22. Double, triple, and quadruple coincidence circuits that operate on either positive or negative input pulses have been built and operated successfully.

The coincidence circuit uses the crystal diode clamp that was first described by Garwin.[6] Another crystal diode clamp, biased in the reverse direction, is introduced in this circuit to improve the discrimination

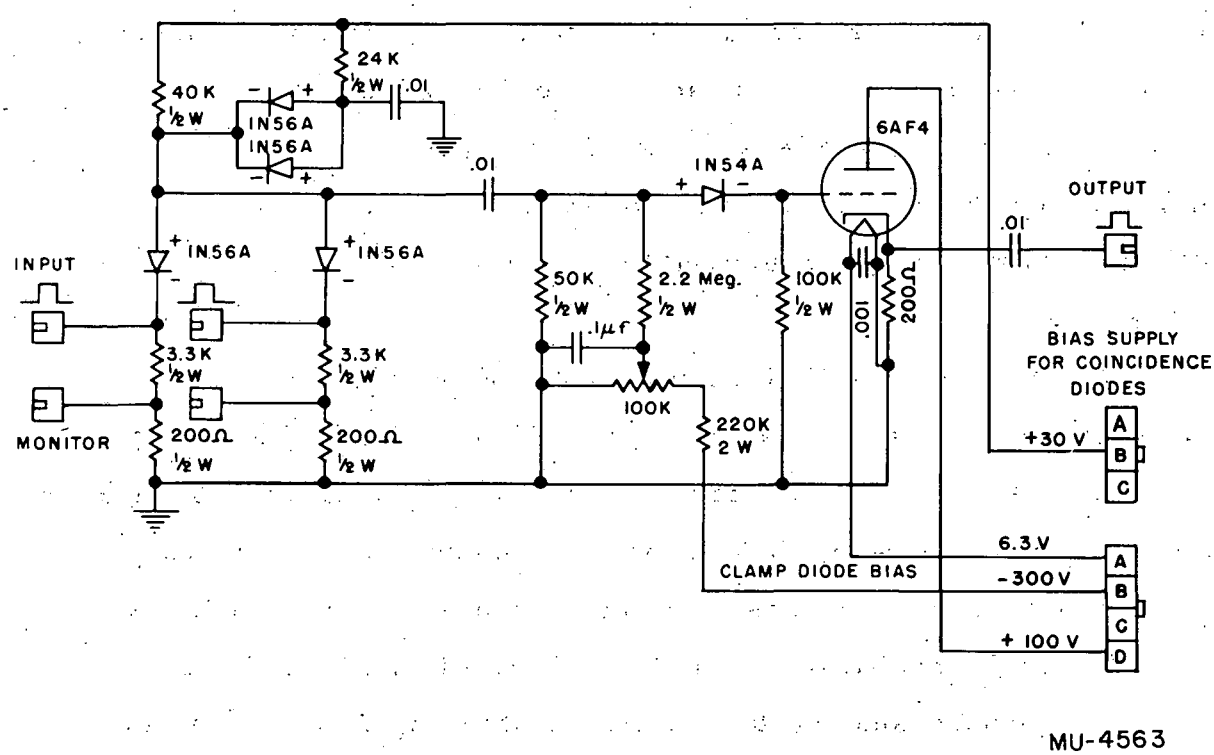

Fig. 19. Crystal diode double-coincidence circuit for positive input pulses.

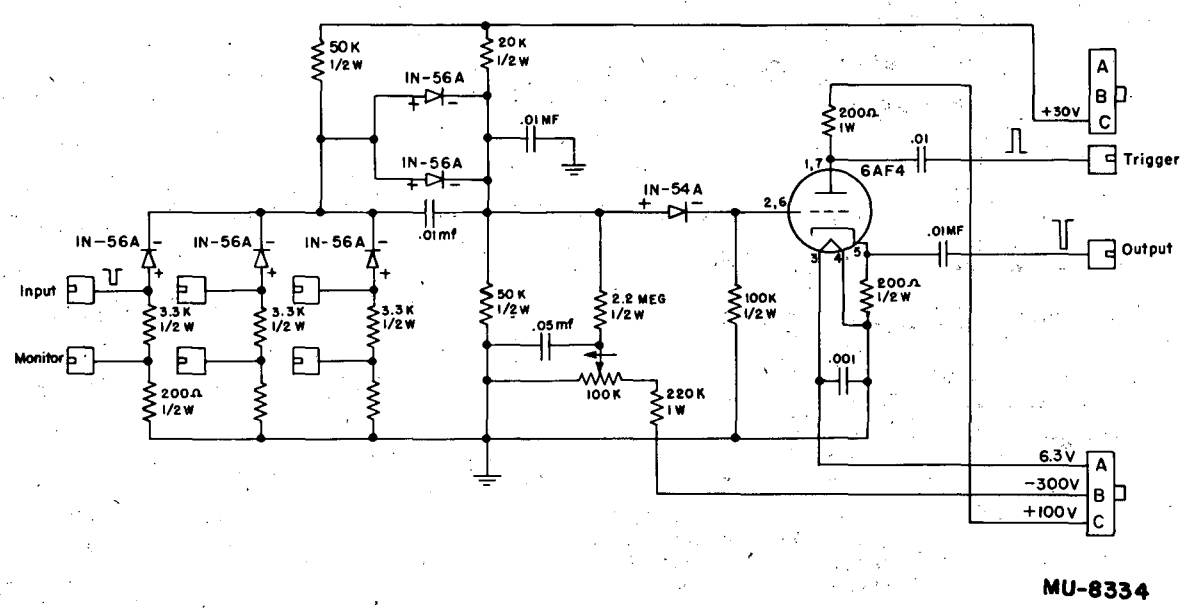

Fig. 20. Crystal diode double-coincidence circuit for negative input pulses.

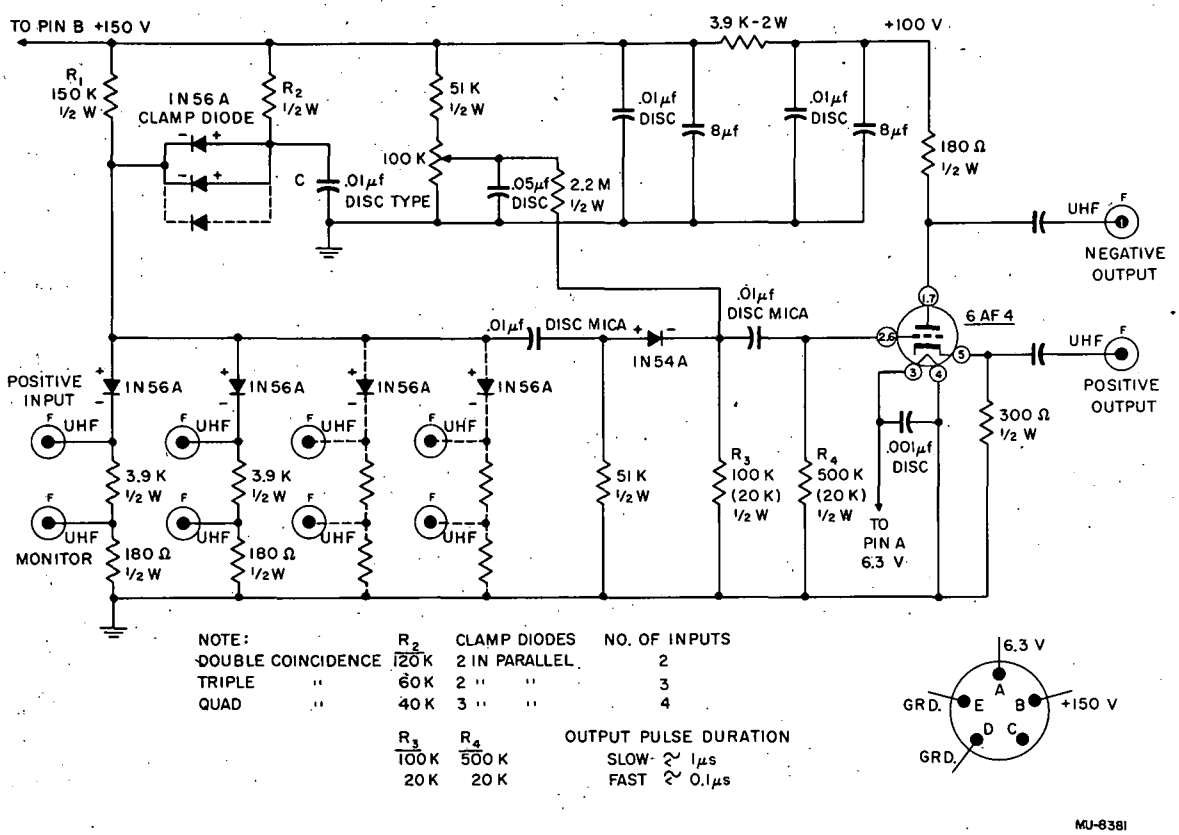

Fig. 21. Crystal diode coincidence circuits for positive input pulses.

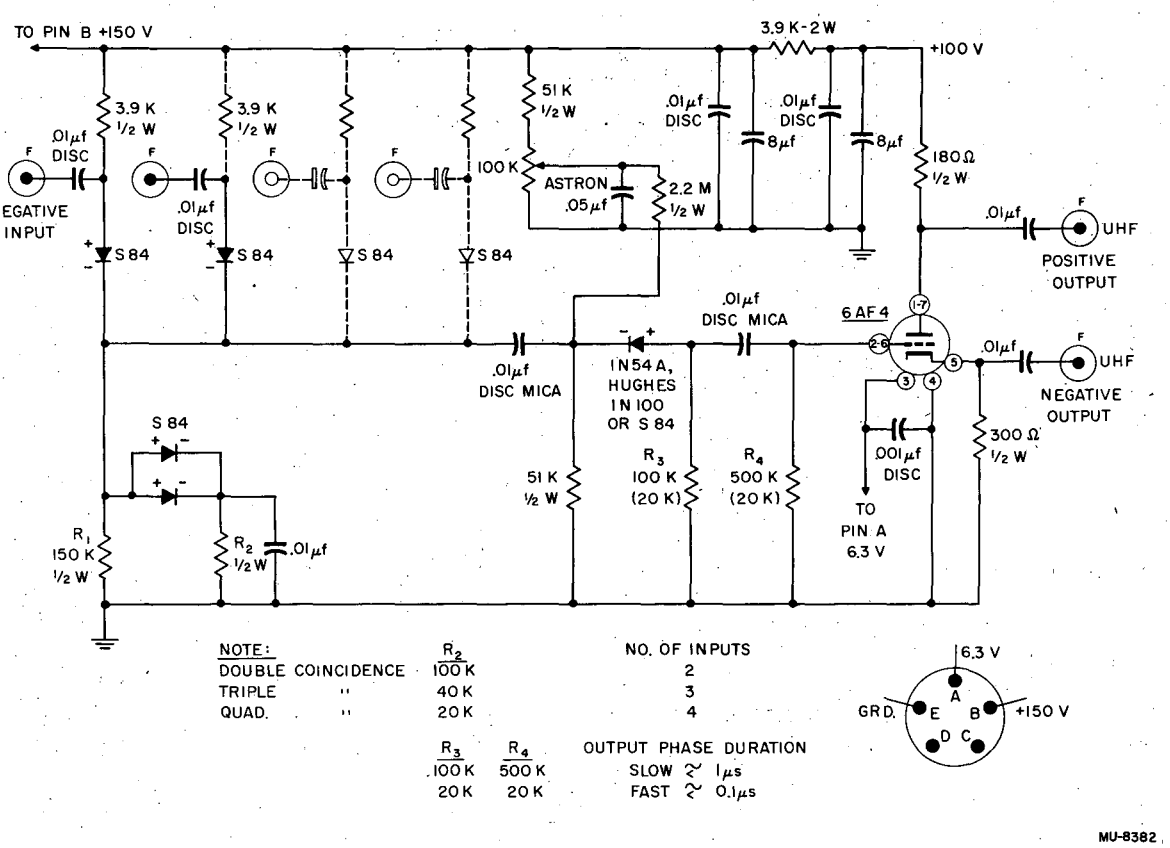

Fig. 22. Crystal diode coincidence circuits for negative input pulses.

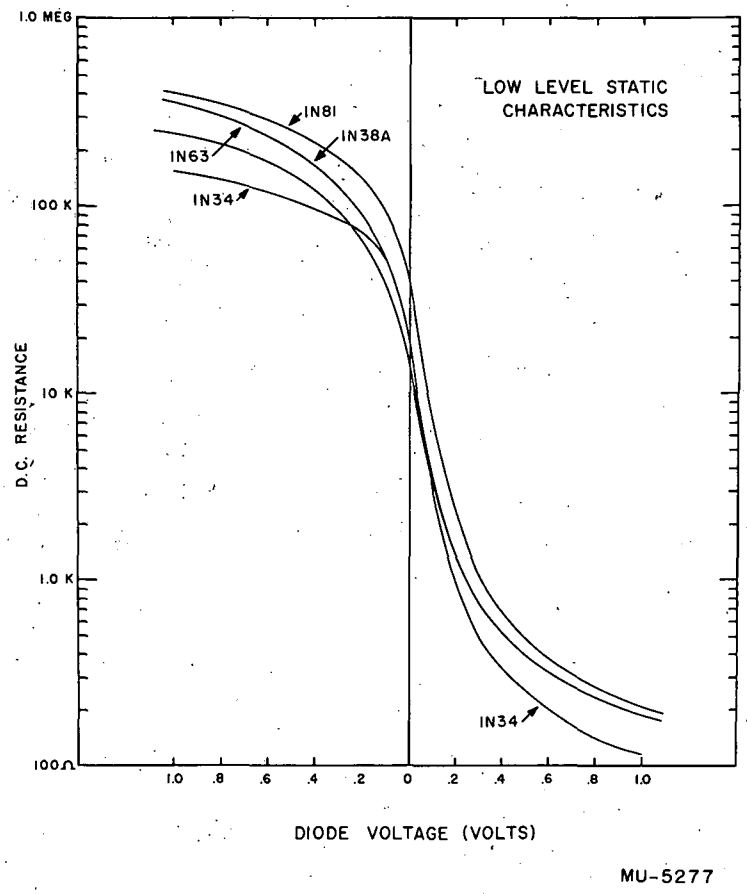

Fig. 23. Low-level static characteristics of crystal diodes.

ratio. Either the type IN54A, the type 1N100, or the type S84 crystal diode is selected for this application because of a very steep back-resistance — versus — back-voltage characteristic at small back voltages. Figure 23 shows the low-level static characteristics of some germanium diodes in the region near minus one volt. The reverse biasing current for this diode is furnished from a nearly constant current source. The reverse bias current is adjusted to give a reverse bias voltage that is smaller in magnitude than the signal voltage that appears at the input end of the back-biased diode in response to coincident input pulses. A typical value of the reversed bias voltage is 0.60 or 0.70 volt. A noncoincident pulse, being smaller than a coincident pulse, is presented by the high back resistance of the diode, so that only a very small fraction of this pulse is transmitted; on the other hand, a coincident pulse is presented with a very small diode resistance so that this pulse is transmitted with little attenuation. The constant-current biasing supply and the 50,000-ohm shunting resistor stabilize the performance of this back-biased diode; however, the magnitude of the reverse bias is still slightly sensitive to fairly large temperature changes. When the circuit is used in open-air areas for a period of several days, the magnitude of the reverse bias voltage is checked periodically for small drifts that can occur. Little or no drift occurs in the reverse bias voltage if the ambient temperature is reasonably constant. Neither crystal diodes nor other components have to be selected to give reliable performance in this coincidence circuit.

A coincidence pulse charges the distributed capacity in the grid circuit of the output tube through the forward resistance of the 1N54A diode. If the back resistance of the diode is large compared to the 100K grid resistor, then the charged capacity discharges to ground through the 100K grid resistor; otherwise, the parallel path to ground through the back resistance of the diode shortens the discharge time. For coincidence

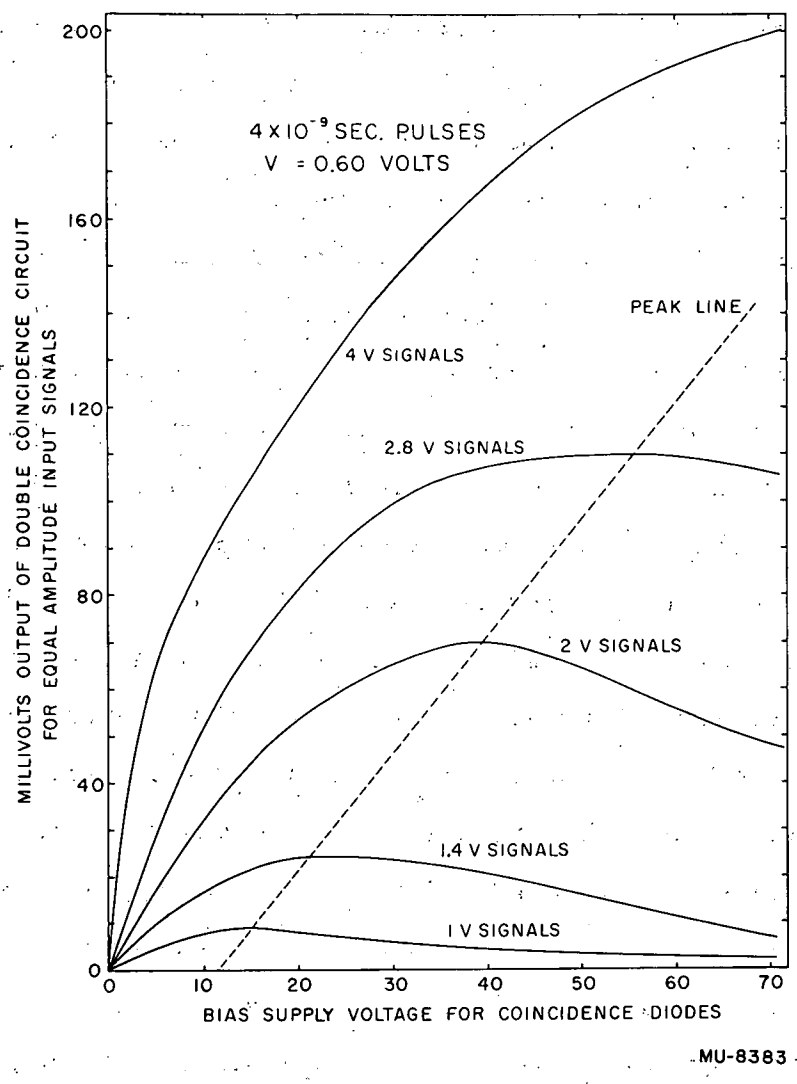

Fig. 24. Double-coincidence output in millivolts versus the bias supply volts for the coincidence diodes when both input signals are equal in amplitude and four millimicroseconds in duration. The amplitude of the negative input signals is indicated on each curve. The reverse bias voltage across the clamp diode is 0.60 volt.

input pulses for four millimicroseconds duration, the decay time of the 6AF4 cathode follower output pulse was observed on an oscilloscope to be a few tenths of a microsecond. The observed decay time is in good agreement with that expected from the RC time constant in the grid circuit.

The performance of the coincidence circuit has been checked with a mercury-switch pulser and a fast oscilloscope. The pulser generated either positive or negative pulses of four-millimicrosecond duration or longer; the pulse duration is measured at the base of the pulse. The rise time of the pulses, after passing through resistance attenuators, was about 1.5 millimicroseconds; thus the pulse would rise to full amplitude in 1.5 millimicroseconds, remain flat for 1 millimicrosecond, and then decay to zero in 1.5 millimicroseconds. The voltage from each of four outputs of the pulser could be switched in convenient steps from 5 millivolts to 80 volts.

Figures 24 through 30 are the results of tests on the negative input double-coincidence circuit of Fig. 20. These tests were made with the four-millimicrosecond pulses from the pulse generator that was described above. The reverse bias voltage across the clamp diode was fixed at 0.60 volt. The double coincidence output is plotted in Fig. 24 against the bias supply voltage for the coincidence diodes when both input signals are equal in amplitude. The amplitude of the input signals is indicated on each curve. The dotted line passes through the broad peaks of the curves. The same data are presented in a different form in Fig. 25. Here, the double-coincidence output is plotted against the amplitude of one of the two equal-amplitude signals. Each curve is for a different value of supply voltage for the coincidence diodes. The two Figs. 26 and 27 are similar to Fig. 24, except that here one input signal is held fixed at either 20 volts or 2 volts and the other input signal is varied in convenient steps from 5 millivolts up to 800 millivolts. The double-coincidence output

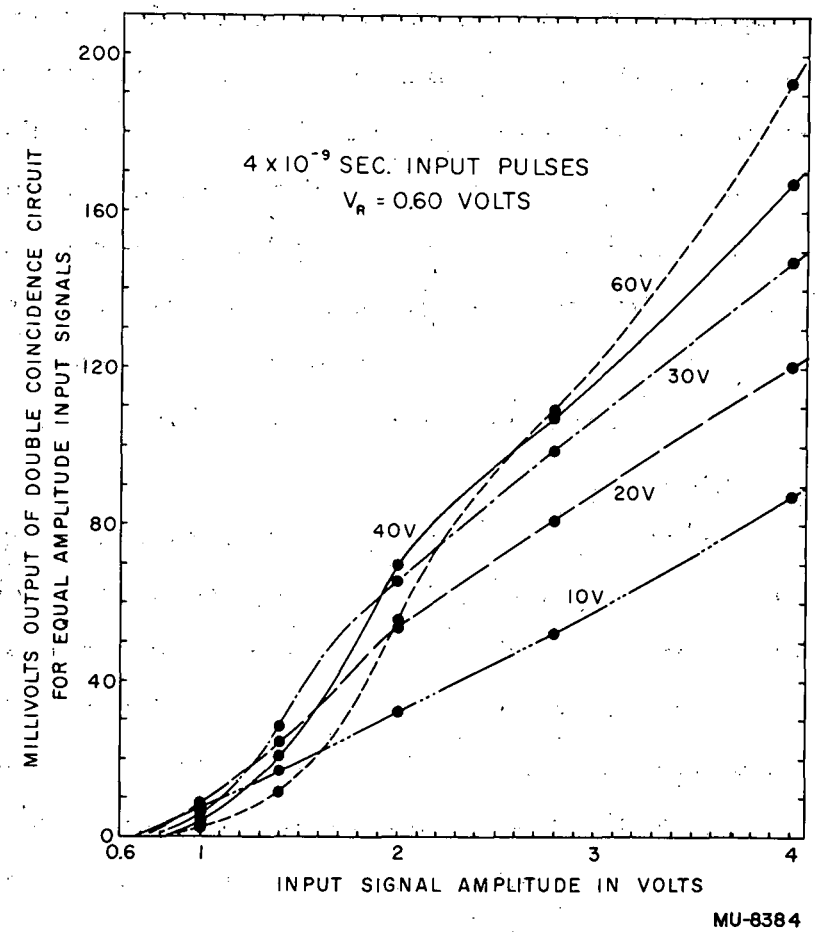

Fig. 25. Double-coincidence output in millivolts versus the amplitude of one of two equal-amplitude, four-millimicrosecond negative input signals. Each curve is for a different value of the bias supply voltage for the coincidence diodes. The reverse bias voltage across the clamp diode is 0.60 volt.

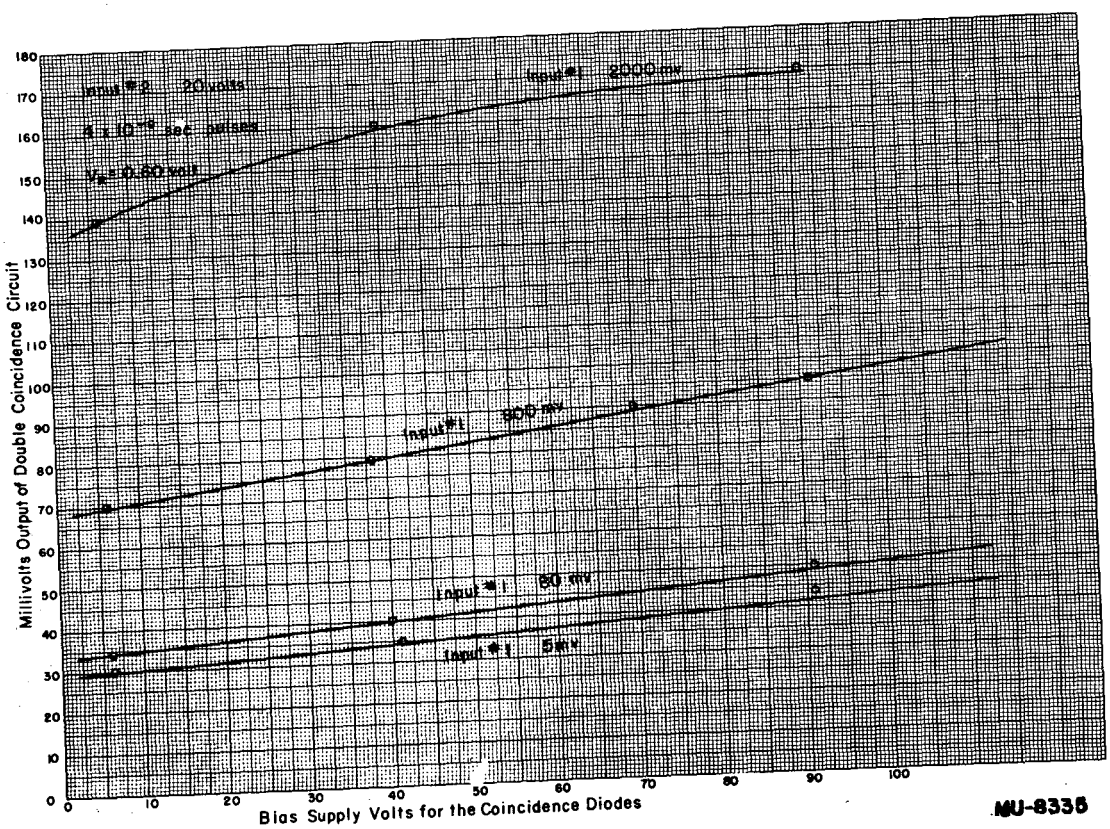

Fig. 26. Double-coincidence output in millivolts versus the bias supply volts for the coincidence diodes when one input signal is held constant at 20 volts and the other is varied in steps from five millivolts to two volts. Each curve is labeled with the amplitude of the four-millimicrosecond signal. The reverse bias voltage across the clamp diode is 0.60 volt.

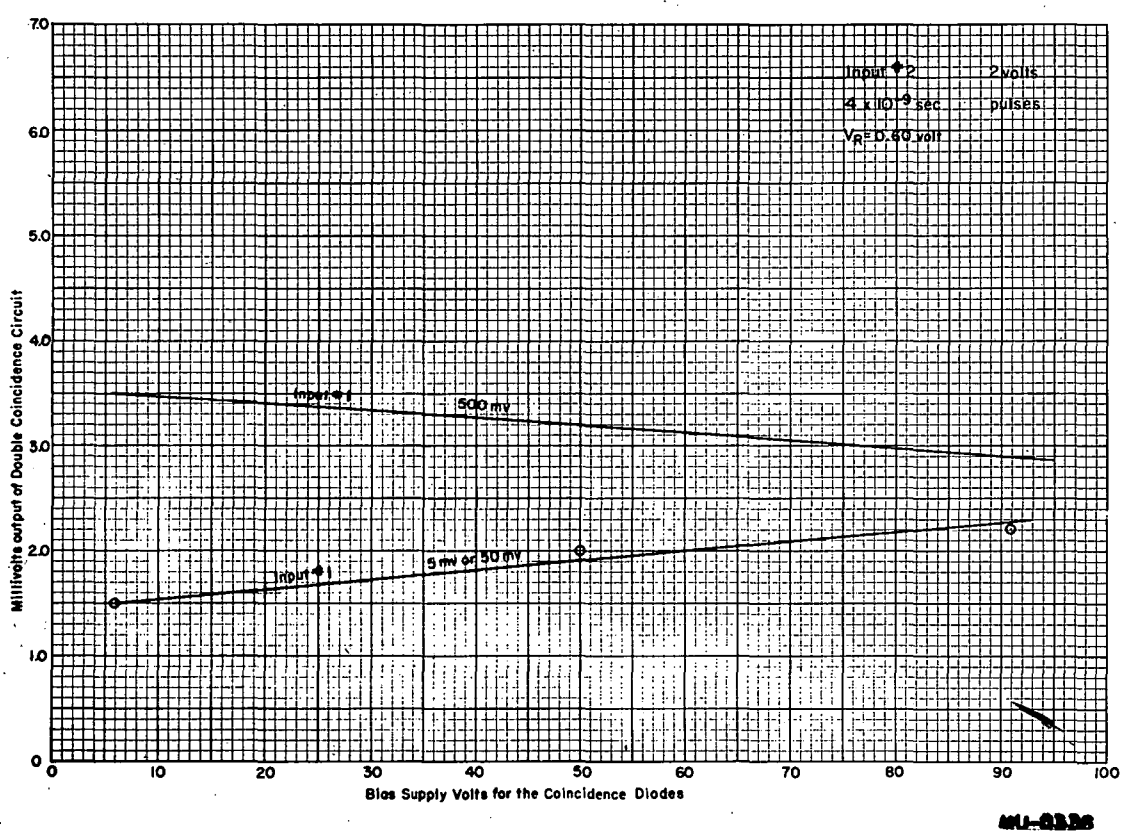

Fig. 27. Double-coincidence output in millivolts versus the bias supply volts for the coincidence diodes when one input signals is held constant at the two volts and the other is varied in steps from five millivolts to two volts. Each curve is labeled with the amplitude of the four-millimicrosecond signal. The reverse bias voltage across the clamp diode is 0.60 volt.

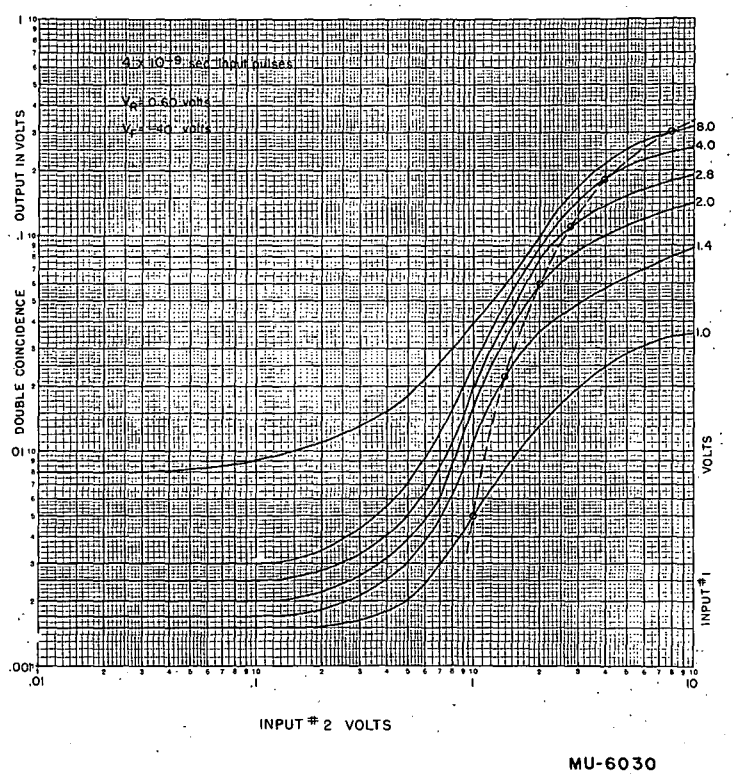

Fig. 28. Double-coincidence output voltage versus the amplitude of one of the input signals when the amplitude of the other input signal is held constant. The negative input signals are four millimicroseconds in duration. The dotted curve is the locus of equal-amplitude signals. The bias supply voltage for the coincidence diodes is minus 40 volts. The reverse bias voltage across the clamp diode is 0.60 volt.

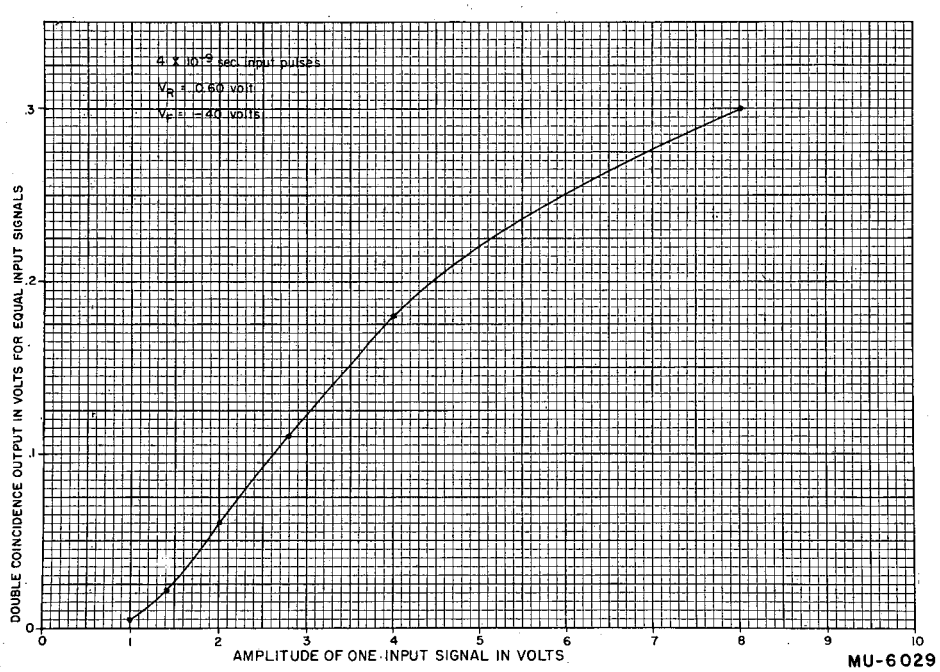

Fig. 29. Double coincidence output voltage versus the amplitude of one of two equal-amplitude, four-millimicrosecond input signals. The bias supply voltage for the coincidence diodes is minus 40 volts. The reverse bias voltage across the clamp diode is 0.60 volt.

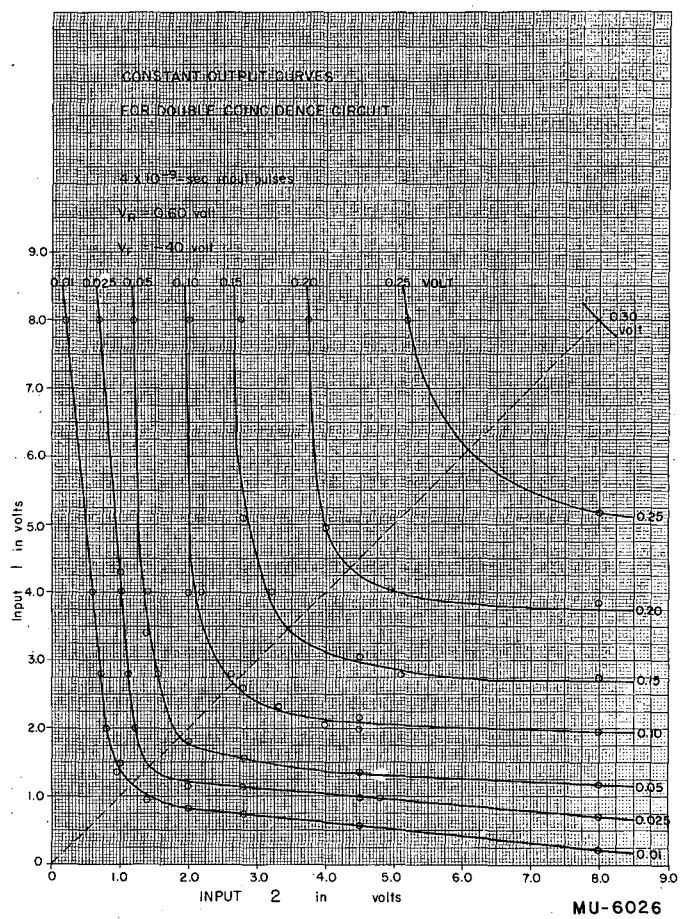

Fig. 30. The amplitude of one input signal versus the amplitude of the other input signal to the double-coincidence circuit for constant output voltage. Each curve is labeled with the amplitude of the output voltage. The negative input signals are four millimicroseconds in duration. The bias supply voltage for the coincidence diodes is minus 40 volts. The reverse bias voltage across the clamp diode is 0.60 volt.

under these conditions shows the "feed-through" level. Each of these curves shows that the feed-through output for a given pair of input signals is relatively insensitive to the bias supply voltage for the coincidence diodes.

The remaining tests were made with a fixed value of 40 volts for the bias supply voltage for the coincidence diodes. This choice corresponds to the maximum value of the curve in Fig. 24 for 2.0-volt input signals. Since the feed-through level, as shown in Fig. 27, is fairly flat, this choice gives a maximum discrimination ratio for 2.0-volt input signals. The discrimination ratio of the double-coincidence circuit for input signals of a given amplitude is here defined as the ratio of the coincidence output for two coincident equal-amplitude input signals to the output of the coincidence circuit for completely nonoverlapping signals of the same amplitude.

Figure 28 is a log-log plot of the double-coincidence output voltage versus the amplitude of one of the input signals when the amplitude of the other input signals is held constant. The dotted curve is the locus of equal-amplitude signals. The curve for equal-amplitude input signals is plotted with linear scales in Fig. 29. Note that the double-coincidence output is plotted here against the amplitude of only one of the two equal-amplitude input signals. The data of Fig. 28 are displayed in another form in Fig. 30. Here, lines of constant output voltage are plotted on a grid where the amplitude of one input signal is represented along the ordinate and the amplitude of the other input signal along the abscissa.

IV. OUTPUT CIRCUITS

The output pulse from the coincidence circuit is still too fast and too small for reliable operation of the discriminator circuit in the standard Radiation Laboratory scalers. A fast amplifier amplifies the negative output pulse to a level that reliably operates another crystal diode pulse-lengthening circuit. The circuit diagram of a satisfactory pulse-lengthening amplifier is given in Fig. 31. The first stage of this circuit consists of an EEP-60 secondary emission tube amplifier. The high g_m/C ratio, where g_m is the transconductance and C is the input capacitance, for this tube results in a good high-frequency response. Negative feedback is employed from plate to grid. The output signal to the next stage is taken from the dynode. The pulse-lengthening diode, in the grid circuit of the 6AQ5 pentode amplifier stage, is poled to lengthen negative pulses. Since the dynode has the property of not inverting the polarity of the input grid pulse, the circuit of Fig. 31 is driven by negative pulses. An output pulse of either polarity can be taken from the 6AF4 output tube of the coincidence circuit. The negative grid drive and dynode coupling reduces overload paralysis of the amplifier. Large negative signals on the first two grids can only drive the tubes beyond cutoff; large positive signals would draw grid current which could prevent the amplifier from responding properly to a successive pulse until the effect of excessive grid current has subsided. The output tube is a triode-connected 6AQ5 cathode follower. The cathode follower is driven in the positive direction in order to obtain a larger output swing than one that is driven in the negative direction and that operates from the same power supply. The low-impedance output of the cathode follower is required in order to drive long lengths of coaxial cable from the experimental area to the counting area. The output-input relationship of this amplifier for 0.1 microsecond input pulses is given in Fig. 32. The log-log plot shows both the linear range and the saturation range. The dotted curve gives the amplitude of a second pulse that appears at the output when the input is excessively overloaded.

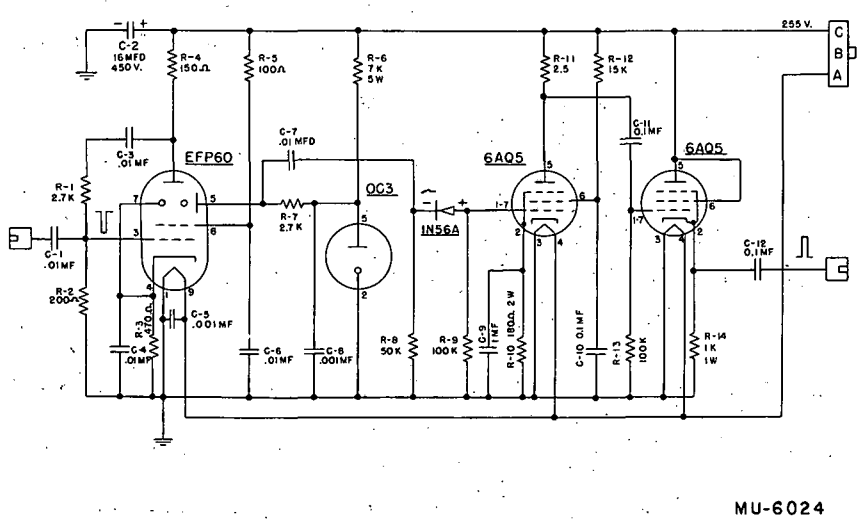

Fig. 31. Pulse-lengthening amplifier for negative output pulses from the coincidence circuit.

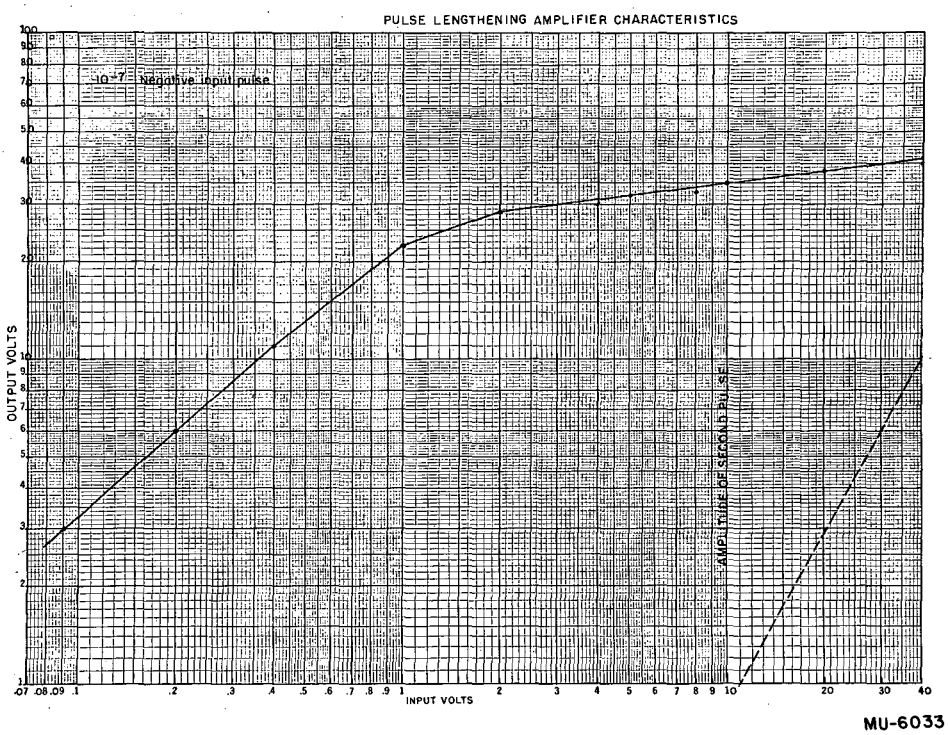

Fig. 32. The output pulse height from the pulse-lengthening amplifier versus the negative amplitude of a one-tenth-microsecond input pulse.

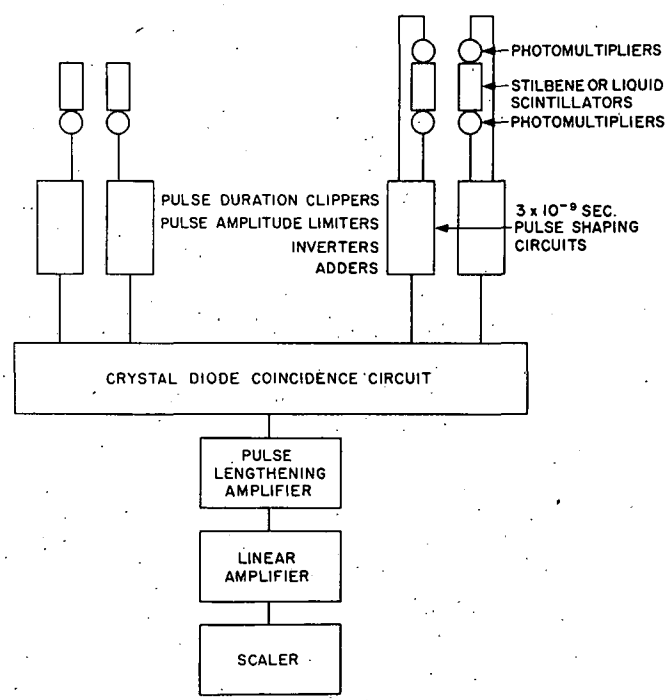

A TYPICAL FAST COUNTING SETUP

MU-5276

Fig. 33. The pulse-shaping and coincidence system.

V. OVER-ALL PERFORMANCE OF THE COINCIDENCE SYSTEM

The over-all performance of the coincidence system has been observed under varying conditions. The coincidence system in Fig. 33 has been tested with the same four-millimicrosecond pulses from the mercury-switch pulser that was described briefly in Section V. In Fig. 34, the discriminator bias in volts is plotted against the amplitude of one of two equal input pulses to the coincidence system of Fig. 35. The 197-ohm clipping lines in the grids of the adder circuit (Fig. 6) have been disconnected for this test. The negative input doubles circuit is operated with a bias supply voltage of minus 40 volts for the coincidence diodes and with a reverse bias voltage of 0.60 volt across the clamp diode. The output linear amplifier was set at minimum gain. The 1/e-decay time for the output pulse from the linear amplifier was observed to be about seven microseconds. Note that the output pulse height of the system in the microsecond range is a linear function of the amplitude of one of two equal input pulses in the millimicrosecond range.

The resolution function of the triple-coincidence system for equal amplitude input pulses is given in Fig. 35. Each curve has been taken for a different value of input pulse amplitude. The linear amplifier output in volts is plotted as a function of the length in feet of 197-ohm delay line in one input to the triple-coincidence circuit of Fig. 35. One foot of this cable is equivalent to a delay time of 1.068 millimicroseconds. (See Table III). The negative input pulses from the mercury-switch pulser have a rise time of about 1.5 millimicroseconds and a duration at the base of the pulse of four millimicroseconds. The negative-input triple-coincidence circuit is operated with a bias supply voltage of minus 60 volts and with a bias voltage of 0.60 volt across the type 1N54A diode.

The efficiency of the fast counting equipment for the detection of protons that lose about 8 Mev in stilbene phosphors was measured[7] at the Berkeley 184-inch synchrocyclotron. Four stilbene phosphors, each

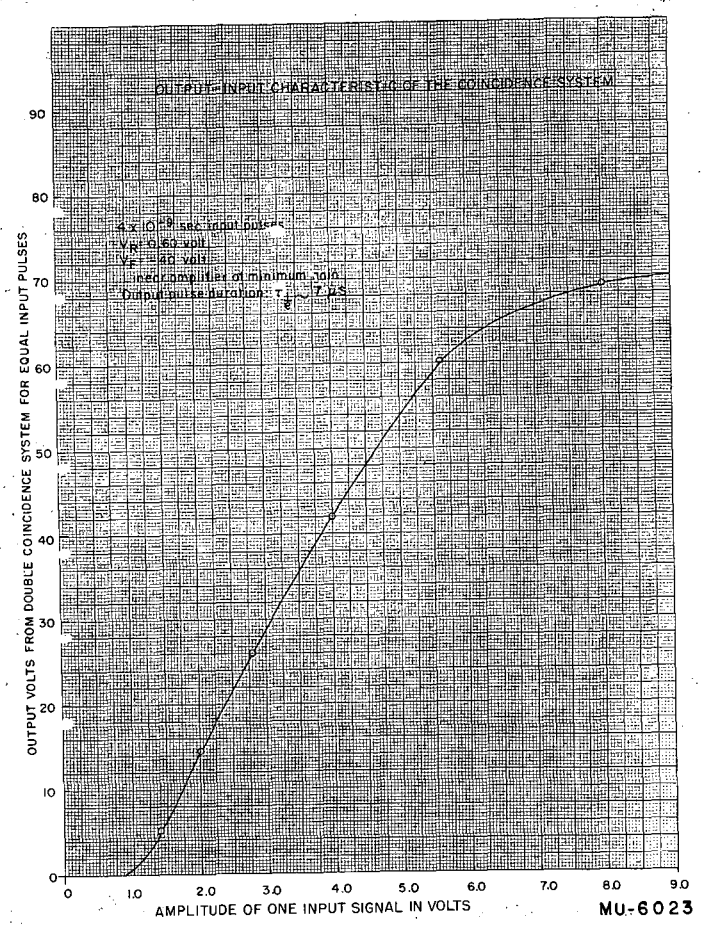

Fig. 34. Discriminator bias in volts versus the amplitude of one of two equal input pulses to the system of Fig. 35. The positive input pulses from the mercury-switch pulser are four millimicroseconds in duration. The 197-ohm clipping lines in the adder circuit (Fig. 6) have been discontinued for this test. The negative input double-coincidence circuit (Fig. 20) is operated with a bias supply voltage of minus 40 volts for the coincidence diodes and with a reverse bias voltage of 0.60 volt across the clamp diode. The linear amplifier was set at minimum gain. The 1/e-decay time for the pulse from the linear amplifier was about seven microseconds.

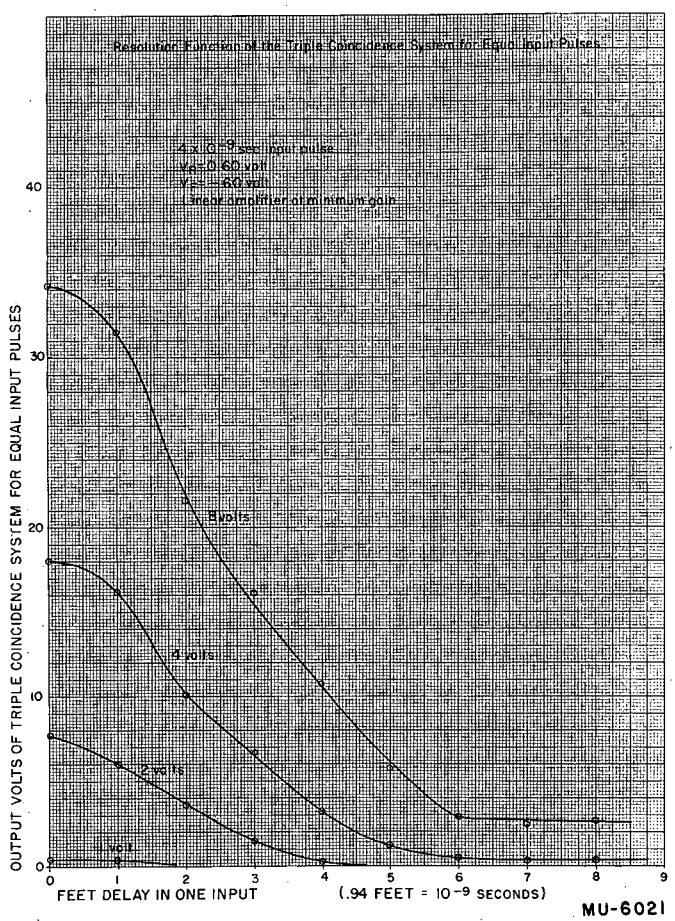

Fig. 35. Resolution function of the triple-coincidence circuit for equal-amplitude input pulses. Each of the curves is labeled with a particular value of input pulse height. Linear-amplifier output in volts for minimum linear-amplifier gain versus the length in feet of 197-ohm delay line in one input to the triple-coincidence circuit of Fig. 22. One foot of this cable is equivalent to a delay time of 1.068 millimicroseconds. The linear amplifier was set at minimum gain. The negative input pulses from the mercury-switch pulser are four millimicroseconds in duration. The negative input triple-coincidence circuit is operated with a bias supply voltage of minus 60 volts and with a bias voltage of 0.60 volt across the type 1N54A clamp diode.

2.4 g/cm^2 thick, were aligned in the 340-Mev scattered deflected external proton beam. The phosphors were viewed by 1P21 photomultiplier tubes. The protons were collimated both fore and aft of the steering magnet. The jaws of the premagnet collimator were closed down to 0.10 inch by 0.10 inch. The 40-inch-long brass collimating tube was 0.25 inch in diameter. Photographs were taken to ascertain that the beam passed through the centers of the 3.25-square-inch phosphors. The proton beam intensity was reduced to about five protons per second by operating the source at reduced arc voltage, reduced tank-filament current, and reduced filament voltage. Alternate counters were connected in double coincidence through similar pulse-shaping circuits. The negative collector pulse from the 1P21 photomultiplier is limited in amplitude if the 6BQ7 limiter grid is driven beyond cutoff. The output of each positive-input crystal-diode coincidence circuit was fed through a pulse-lengthening amplifier and a linear amplifier to a discriminator circuit. The output of each discriminator circuit was recorded on a scaler. In addition, if the discriminator circuit is tripped by the output pulse from a fast coincidence circuit, a shaped pulse of constant amplitude and duration is generated. These shaped pulses are fed into a slow double-coincidence circuit D_3. The efficiency of this slow double-coincidence circuit D_3 is assumed to be 100 percent for the detection of these shaped pulses in the microsecond range. If ε_1 and ε_2 are the detection efficiencies of Channels 1 and 2 respectively, then

$$D_1 = \varepsilon_1 N$$

$$D_2 = \varepsilon_1 N$$

$$D_3 = \varepsilon_1 \varepsilon_2 N$$

where D_1 and D_2 are the numbers of fast double coincidences recorded in Channels 1 and 2 respectively. D_3 is the number of slow double coincidences, and N is the number of true coincidence counts. We measure D_1, D_2, and D_3 and solve for the three unknowns ε_1, ε_2, and N.

The results of this measurement are expressed in Figs. 36 and 37. The absolute detection efficiency for protons losing 8 Mev in each stilbene phosphor is plotted against the length of delay line. The shift of the peak of this resolution function to the right of zero delay line is the effect of the proton time of flight between the counters. The detection efficiency is nearly 100 percent around the peak. This measurement has not been corrected for nuclear attenuation of the protons in the stilbene scintillators. The few-percent efficiency loss can be attributed to this cause. The proton beam diameter and the geometry of the counters were such that multiple scattering losses were negligible. The resolving time τ, defined as one-half the full width at half maximum, is just about five millimicroseconds in Fig. 36 and three millimicroseconds in Fig. 37. The detection efficiencies of the triple- and quadruple-coincidence channels are the same as for the double-coincidence channel.

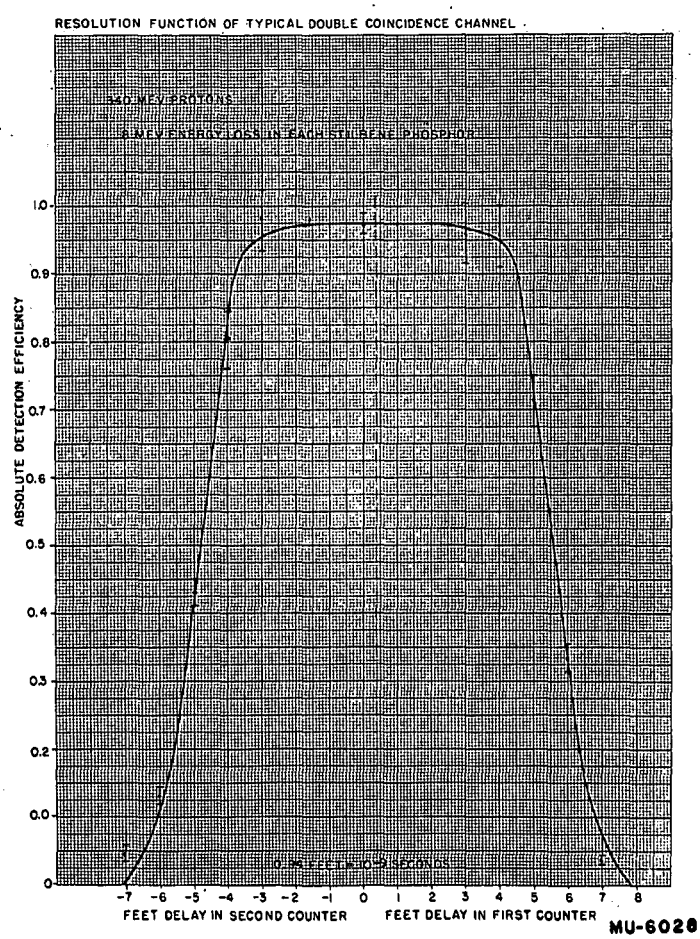

Fig. 36. Resolution function of a typical double-coincidence channel for equal-amplitude input pulses. The amplitude of each input pulse corresponds to an 8-Mev energy loss by 340-Mev protons passing through each stilbene phosphor.

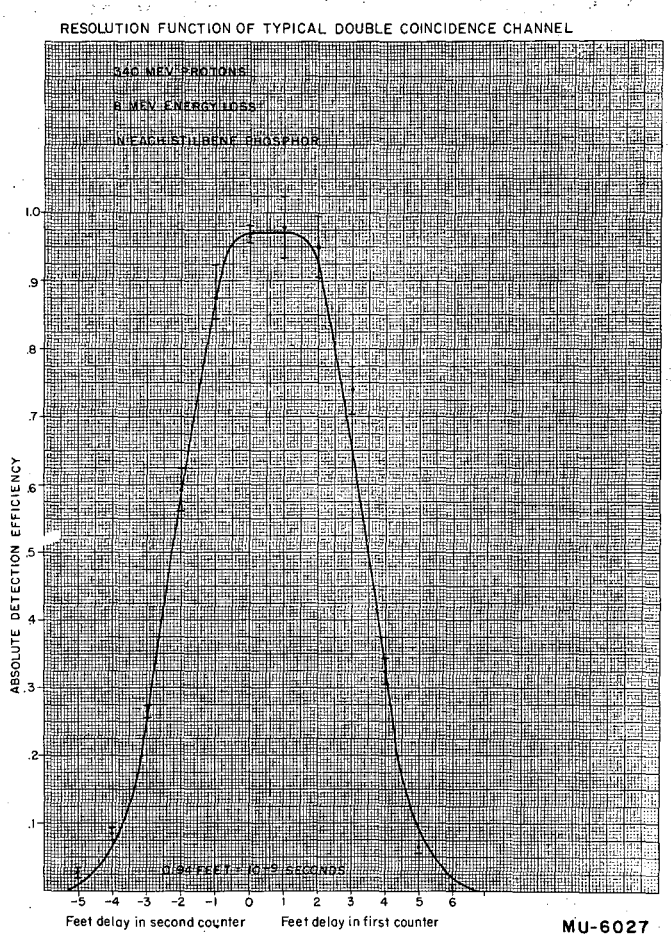

Fig. 37. Resolution function of a typical double-coincidence channel for equal-amplitude input pulses. The amplitude of each input pulse corresponds to an 8-Mev energy loss by 340-Mev protons passing through each stilbene phosphor.

ACKNOWLEDGMENTS

It is a pleasure to acknowledge the contributions of several people during the course of this work. My colleagues, Dr. Kenneth C. Bandtel and Dr. Wilson J. Frank, carried out many of the performance tests; Mr. Richard Mitchell and Mr. David Larson assisted with numerical calculations and with preparation of some of the figures; and Mr. Paul V. Nikonenko was responsible for most of the construction and engineering design. Finally, I would like to express my appreciation to Dr. Burton J. Moyer for his interest, encouragement, and support of this instrumentation and development program.

This work was performed under the auspices of the U. S. Atomic Energy Commission.

REFERENCES

1. W. J. Frank, K. C. Bandtel, R. Madey, and B. J. Moyer, Phys. Rev. 94, 1716 (1954).

2. H. B. Phillips and R. K. Swank, "Measurements of Scintillation Lifetimes," Rev. Sci. Instr. 24, 611 (1953).

3. C. J. Taylor, W. K. Jentschke, M. E. Remley, F. S. Eby, and P. G. Kruger, Phys. Rev. 84, 1034 (1951).

4. J. B. Birks, Scintillation Counters, McGraw-Hill (1953).

5. B. Rossi, Nature 125, 636 (1930).

6. R. L. Garwin, Rev. Sci. Instr. 21, 569 (1950).

7. R. Madey, K. C. Bandtel, and W. J. Frank (unpublished).